JP9950004

JAERI-Tech
98-060

ANALYSIS OF THE HTTR'S BENCHMARK PROBLEMS AND COMPARISON BETWEEN THE HTTR AND THE FZJ CODE SYSTEMS

January 1999

Nozomu FUJIMOTO, Ursula OHLIG*
Hans BROCKMANN* and Kiyonobu YAMASHITA

日本原子力研究所
Japan Atomic Energy Research Institute

本レポートは、日本原子力研究所が不定期に公刊している研究報告書です。
入手の問合わせは、日本原子力研究所研究情報部研究情報課（〒319-1195　茨城県那珂郡東海村）あて、お申し越しください。なお、このほかに財団法人原子力弘済会資料センター（〒319-1195　茨城県那珂郡東海村日本原子力研究所内）で複写による実費頒布をおこなっております。

This report is issued irregularly.
Inquiries about availability of the reports should be addressed to Research Information Division, Department of Intellectual Resources, Japan Atomic Energy Research Institute, Tokai-mura, Naka-gun, Ibaraki-ken 319-1195, Japan.

編集兼発行　日本原子力研究所

JAERI-Tech 98-060

Analysis of the HTTR's Benchmark Problems and Comparison between the HTTR and the FZJ Code Systems

Nozomu FUJIMOTO, Ursula OHLIG*
Hans BROCKMANN* and Kiyonobu YAMASHITA

Department of HTTR Project
Oarai Research Establishment
Japan Atomic Energy Research Institute
Oarai-machi, Higashiibaraki-gun, Ibaraki-ken

(Received December 10, 1998)

The first Research Coordination Meeting for the Coordinated Research Program on the HTTR benchmark problems were held in August 1998. The results and calculation models of JAERI and Forshcungszentrum Jülich GmbH (FZJ) by diffusion calculation were compared. Both results showed a good agreement at fully-loaded core but the results of JAERI showed about 1%Δk higher value during fuel loading state. To investigate the cause of the difference, effects of energy group number, neutron streaming from control rod insertion holes and cell models of burnable poison (BP) were studied. As the results, we found that the difference caused by energy group number and neutron streaming were small. The effect of BP cell model was evaluated by sensitivity analysis of dimension of BP cell. Improvements for each calculation model were proposed.

Keywords : HTGR, HTTR, Burnable Poison, Diffusion Calculation, Neutron Streaming, Reactivity, Criticality Tests.

* Forschungszentrum Jülich GmbH

HTTRベンチマーク問題の解析結果とHTTRとFZJのコードシステムの比較

日本原子力研究所大洗研究所高温工学試験研究炉開発部
藤本　望・URSULA OHLIG*・Hans BROCKMANN*・山下　清信

（１９９８年１２月１０日受理）

IAEAの国際協力計画のひとつであるHTTRのベンチマーク問題について、1998年8月の第１回会合で報告された原研とドイツユーリッヒ研究センターの拡散計算モデルとその結果についての比較を行った。その結果、全炉心装荷した状態では良い一致を見たが、燃料装荷途中では原研の結果が約1%Δk高い値を示した。この原因を検討するため、エネルギー群数、制御棒挿入孔からの中性子ストリーミング、反応度調整材のモデルによる効果についての検討を行った。その結果、エネルギー群数及びストリーミングによる差は比較的小さいことがわかった。反応度調整材については、セルモデルの寸法による感度解析を行いその効果を明らかにした。これらの結果を基に、それぞれの解析モデルについて今後の改良項目を提案した。

*　ユーリッヒ研究センター

Contents

1. Introduction 1
2. Characteristics of HTTR 2
3. Outline of Code Systems and Results 5
3.1 HTTR Code System and Results 5
3.1.1 Outline of Calculation Codes 5
3.1.2 Calculation Models and Comparison 6
3.1.2.1 Calculation Models 6
3.1.2.2 Comparison of Models 8
3.1.3 Results of Benchmark Problems 11
3.2 FZJ Diffusion Code System and Results 29
3.2.1 Methods and Data 29
3.2.2 Results of Analysis 30
4. Comparison and Analysis of the Results 45
4.1 Comparison of the Results Obtained by each Code System 45
4.2 Analysis of the Discrepancies in the HTTR and FZJ Results 45
5. Conclusion 55
Acknowledgments 55
References 56

目　　　次

1．はじめに ………………………………………………………………………… 1
2．HTTRの特徴 ……………………………………………………………………… 2
3．コードシステムの概要と比較 …………………………………………………… 5
　3．1　HTTRコードシステムと結果 ……………………………………………… 5
　　3．1．1　コードの概要 ………………………………………………………… 5
　　3．1．2　解析モデルとその比較 ……………………………………………… 6
　　　3．1．2．1　解析モデル ……………………………………………………… 6
　　　3．1．2．2　モデルの比較 …………………………………………………… 8
　　3．1．3　ベンチマーク問題の解析結果 ……………………………………… 11
　3．2　ユーリッヒ研究センターのコードシステムとその結果 ………………… 29
　　3．2．1　方法とデータ ………………………………………………………… 29
　　3．2．2　解析結果 ……………………………………………………………… 30
4．結果の比較と検討 ………………………………………………………………… 45
　4．1　それぞれのコードシステムの結果の比較 ………………………………… 45
　4．2　両コードシステムの間の差異の検討 ……………………………………… 45
5．まとめ …………………………………………………………………………… 55
謝　辞 ………………………………………………………………………………… 55
参考文献 ……………………………………………………………………………… 56

1. Introduction

The start-up core physics experiments of the High Temperature Engineering Test Reactor (HTTR) have been proposed for benchmark problems in the Coordinated Research Program (CRP) of IAEA entitled "Evaluation of HTGR Performance". The proposed benchmark problems are as follows:

1) Number of fuel columns necessary to achieve the first criticality,
2) Control rod positions at criticality of 30 columns, 24 columns and 18 columns core,
3) Excess reactivity of 30 columns, 24 columns and 18 columns core.

The first Research Coordination Meeting (RCM) for the CRP was held on August 1998. When comparing the Japanese and German results presented at the fist RCM, it becomes clear that there are large differences. To clarify the reason of these discrepancies, results and calculational models have been checked each other. The report describes the check of the results, the different calculational models, and some improvements.

2. Characteristics of HTTR

The HTTR is a graphite-moderated and helium gas cooled reactor with an outlet coolant temperature of 950°C and thermal output of 30MW. The characteristics of the HTTR necessary for the benchmark calculations are as follows:

1) Pin-in block type fuel with coated fuel particles

A fuel block consists of 33 or 31 of fuel rods, two burnable poison (BP) rods and a graphite block as shown in Fig. 2.1. Each fuel rod consists of a graphite sleeve and 14 fuel compacts containing coated fuel particles (CFPs). Therefore, it is important to consider the double heterogeneity of the fuel compact.

2) Lumped burnable poison for reactivity control

A BP rod consists of two of BP regions and one graphite region. The BP regions are placed at the top and bottom of the BP rods. The graphite region is placed at the middle of the BP rods. The form of the BP rod is called "zebra type BP rods".

3) Many holes in the core for control rod insertion, etc.

To insert control rods and boron pellets of the reserved shutdown system into the core, there are many holes in the core. It is important to consider neutron streaming effects through these holes.

4) Fuel loading order from outer to inner core region

Before fuel loading, the whole fuel region in the core is filled with graphite dummy blocks. A pile of 9 blocks is called a column. The fuel loading is carried out by replacing the dummy blocks with fuel block, column by column. The fuel loading scheme is shown in Fig.2.2. The fuels are loaded from the periphery to the center, and thin and thick annular cores are made at 18 and 24 fuel-column-loaded core, respectively.

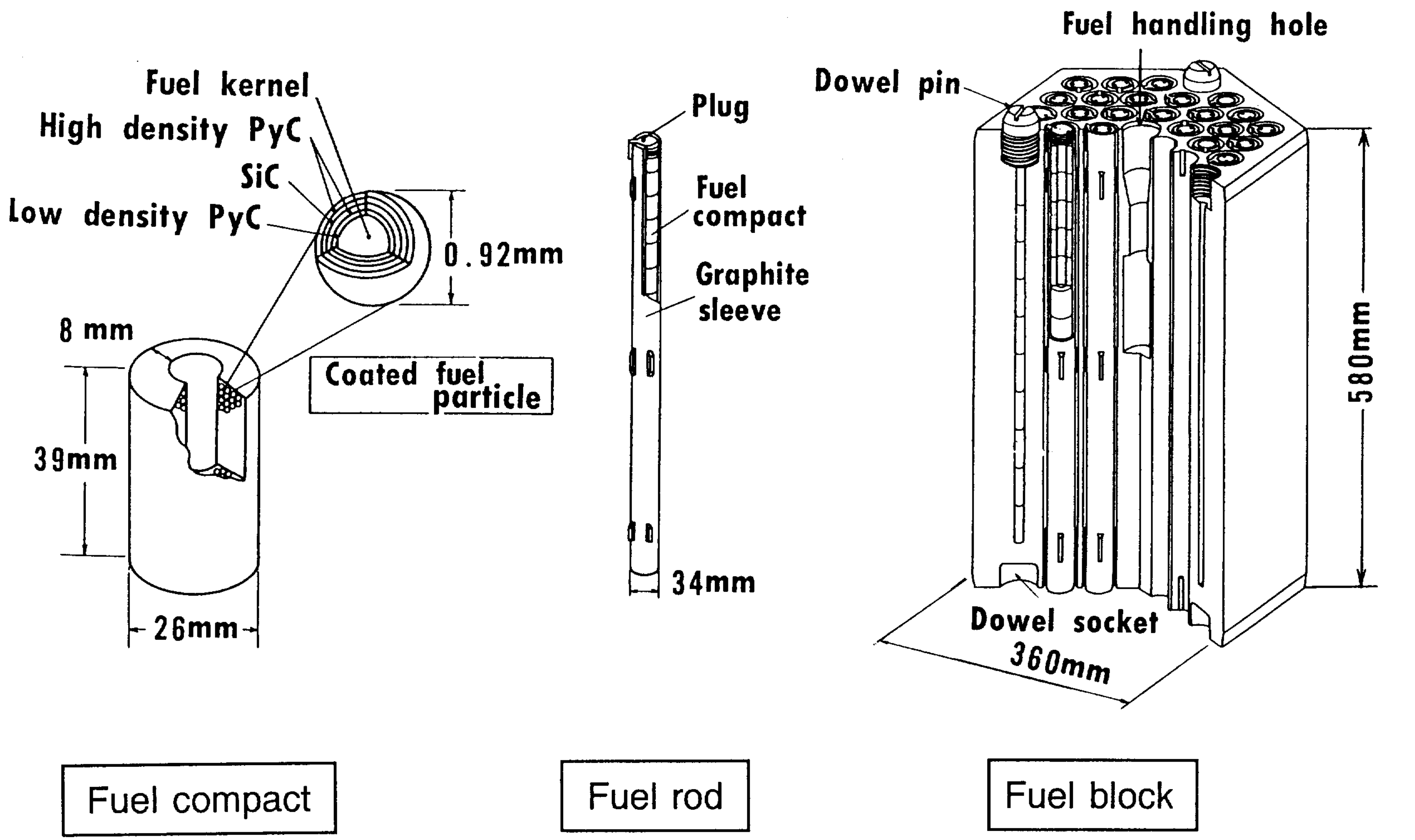

Fig. 2.1 Block type fuel of the HTTR

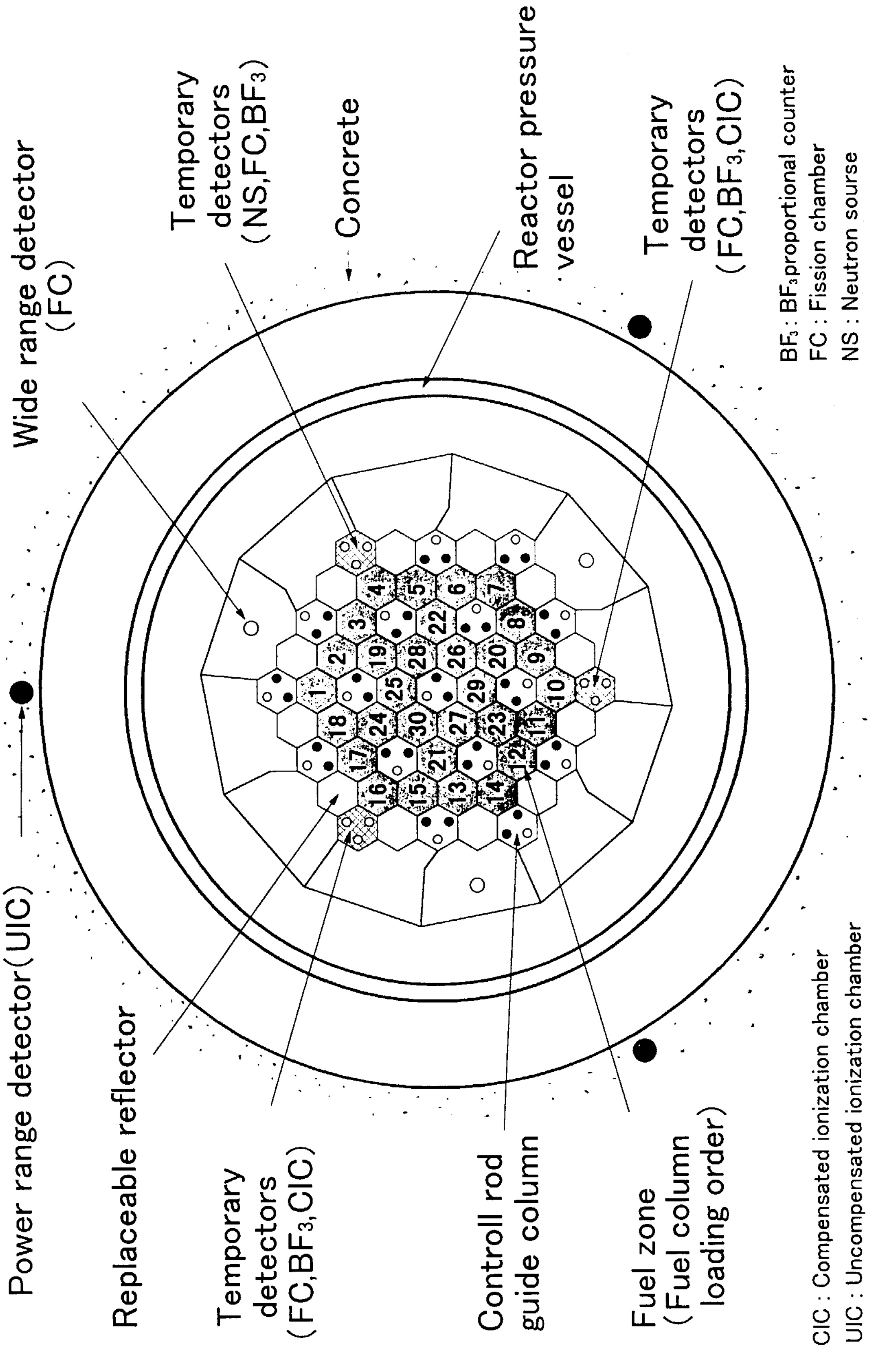

Fig.2.2 Fuel loading shceme of the HTTR

3. Outline of the Code Systems and Results

3.1 HTTR Code System and Results

This chapter describes the improvements of the calculation models, developed at JAERI for the calculations of the HTTR's nuclear characteristics, and the results of the benchmark problems.

3.1.1 Outline of calculation codes

The calculations for the benchmark problems were carried out by a nuclear characteristics evaluation code system which was developed from an HTTR nuclear design code system[1]. The code system consists of the DELIGHT[2], TWOTRAN-II[3] and CITATION-1000VP[4] codes. The program structure of the system is shown in Fig. 3.1.1. The DELIGHT is an one-dimensional lattice burnup cell calculation code that has been developed in the JAERI. The TWOTRAN-II is a transport code that is used to provide the average group constants of BP in fuel blocks and graphite blocks where control rods (CRs) are inserted. The CITATION-1000VP is a reactor core analysis code. This code has been developed from CITATION[5] so that nuclear characteristic analyses could be carried out with a three-dimensional whole core model of the HTTR in a short calculation time.

The DELIGHT is used to provide group constants of fuel and graphite blocks for succeeding core calculations. Resonance, neutron spectrum, neutron flux distribution, criticality, and burnup calculations are done sequentially. Nuclear data are based on ENDF/B-IV except burnup chain data that are extracted from ENDF/B-III. In the resonance range, the code employs intermediate resonance approximation and can consider the effect of a double heterogeneity caused by coated fuel particles (CFPs) and assembled fuel rods. The average group constants of the whole fuel block were obtained by the fuel and BP cell calculations as follows;

First, the group constants of the fuel rods were calculated by using an one-dimensional cylindrical fuel cell model as shown in Fig. 3.1.2. The neutron spectrum was calculated with 111 neutron groups using P_1 approximation for the whole energy range. The group constants were condensed with the neutron spectrum to 40-group constants for neutron flux distribution calculations in the fuel cell. The neutron flux distributions were calculated with the collision probability method, and were used to average the group constants in the fuel cell geometrically.

Second, the average group constants of the fuel block with the BPs were calculated with the one-dimensional cylindrical BP cell model shown in Fig. 3.1.3. The averaging of the group constants in the BP cell was done by the neutron flux in the cell. The group constants were condensed to six-groups by the 40-groups neutron spectrum for the succeeding core calculation.

The TWOTRAN-II was employed to obtain the average group constants of a pair of CRs inserted into the CR guide graphite block and also to obtain the average group constants of zebra type BP. The average group constants of a pair of CRs and of the corresponding graphite block were obtained with the flux-weighting method. The neutron fluxes were calculated with a two-dimensional X-Y model as shown in Fig. 3.1.4. The model is the half of the graphite block where a CR is inserted. The average group constants of zebra type of BP are also evaluated by the TWOTRAN-II code. The models are described later.

The CITATION-1000VP is a reactor core analysis code based on the diffusion theory. This code was changed to enable a full core model calculation of the HTTR by extending the number of zones and meshes of the original CITATION code and enhancing the calculation speed by the vectorization of the code. This code was used for the analysis of the effective multiplication factor. The neutron energy groups consist of 3 fast and 3 thermal groups.

3.1.2 Calculation Models and Comparison

3.1.2.1 Calculation Models

To solve the benchmark problems, three calculation models (6 mesh, 24 mesh and 24 mesh heterogeneous model) were developed. The results of these models were compared. They were also compared with the results obtained by the Monte Carlo code MVP[6]. The MVP code is verified by comparison with VHTRC experiments[7]. All calculations were performed at 300K and 1 atm pressure of helium. Number densities of each components are based on the report[8].

(1) 6 mesh model

A fuel block is divided into 6 triangular meshes horizontally and into 4 meshes vertically for the three-dimensional whole core calculation. Horizontal and vertical cross-section of the calculation model are shown in Fig.3.1.5 and 3.1.6, respectively. In a fuel block, all nuclides are distributed homogeneously. In the CR guide columns, every block is divided into 4 zones vertically to simulate CR insertion depth from full-in to full-out. All group constants are evaluated by the DELIGHT code. The cross section of the fuel cell model is the same as the fuel block cross section divided by the number of fuel rods. The radius of fuel cell shown in Fig. 3.1.2 are as follows: For 33 pin block, R1 is 2 .09 cm and R2 is 3.41 cm. For 31pin block, R1 is 2.10 cm and R2 is 3.52 cm. The radius of the BP cell model is decided to keep the amount of material per BP rod. The R_{BP} shown in fig. 3.1.3 is 16.2 cm. Infinite multiplication factors (k_{inf}) of fuel cell and BP cell for each fuel block are shown in Table 3.1.1.

(2) 24 mesh model

A fuel block is divided into 24 triangular meshes horizontally and into 4 meshes vertically for the three-dimensional whole core calculation to simulate the position of the BP rods in a fuel block. In the horizontal plane, a BP rod is smeared in BP region which consists of two triangular meshes. ^{10}B and ^{11}B in a BP rod are distributed only in the BP region. The other nuclides e.g. uranium, are distributed homogeneously in the whole fuel block. Horizontal and vertical cross-section of the calculation model are shown in Fig. 3.1.7 and 3.1.8, respectively.

All group constants for fuel and graphite are the same as those in the 6 mesh model. Absorption microscopic cross section (σ_a) of ^{10}B in BP rod is evaluated by TWOTRAN-II code to evaluated the zebra type BP. Three kinds of σ_a are evaluated. The first one is for the fuel block with 7.9% enrichment of ^{235}U, 33 fuel pins and 2.0wt% of boron concentration in the BP rods. This σ_a-set is used for all BPs in the first layer of fuel blocks. The second one is for the fuel block with 6.3% enrichment of ^{235}U, 33 fuel pins and 2.5wt% of boron concentration in the BP rods which is used for all BPs with 2.5wt% of boron concentration. The third one is for the fuel block with 3.9% enrichment of ^{235}U, 33 fuel pins and 2.0wt% of boron concentration in the BP rods. This kind of σ_a is used for all BPs in the 4th and 5th layer of fuel blocks. Table 3.1.2 shows the k_{inf} of BP cell calculated by TWOTRAN-II. The corresponding k_{inf} of the fuel cell are also shown in Table 3.1.2 for reference. The σ_as are obtained with the flux-weighting method. The neutron fluxes were calculated in 6 energy groups with a two-dimensional r-Z model as shown in Fig. 3.1.9 The BP cell is modeled for a quarter of a fuel block which contains half of the BP rod. The BP rod consists of BP pellets and C pellets which are surrounded by homogenized fuel. In order to obtain the effective microscopic cross section, a homogenized region is determined having the same area of the BP region as in the CITATION-1000VP model.

(3) 24 mesh heterogeneous model

In this model, the three-dimensional mesh for CITATION-1000VP is the same as that in the case of the 24 mesh model. A fuel block is divided into BP region and fuel region as shown in Fig. 3.1.10. ^{10}B and ^{11}B in a BP rod are distributed only in the BP region. Nuclides of the fuel are distributed only in the fuel region.

All group constants for fuel and graphite are evaluated by the DELIGHT code. The cross section of a fuel cell model is the same as those of the fuel region cross section divided by the number of fuel rods, but the fuel region cross section is 20/24 of the cross section of the fuel block. Therefore, the outer radius of this cell model is smaller than the other ones. The radius of fuel cell shown in Fig. 3.1.2 are as follows: For 33 pin block, R1 is 2.09 cm and R2 is 3.11 cm. For 31 pin block, R1 is 2.10 cm and R2 is 3.21 cm.

Three kinds of σ_a for ^{10}B in the BP rod are also evaluated by TWOTRAN-II code. The evaluated σ_as are the same as those taken for the 24 mesh model. The BP cell model corresponds to a quarter of a fuel block which contains half of the BP rod is shown in Fig. 3.1.11. The BP rod consists of BP pellets and C pellets which are surrounded by graphite, the outer region contains homogenized fuel. In order to obtain the effective microscopic cross section, a homogenized region is determined to have the same cross section as the BP region in the CITATION-1000VP model. Table 3.1.3 shows the k_{inf} of fuel and BP cell calculated by the DELIGHT and TWOTRAN-II, respectively. The k_{inf}-values of the fuel cell obtained by TWOTRAN-II are also shown for comparison.

3.1.2.2 Comparison of Models

To evaluate the characteristics of each model, the following effects are examined.

(1) Mesh effect

The effect of mesh size is evaluated by 6 mesh per block and 24 mesh per block. Table 3.1.4 shows the comparison of k_{eff} at 18 column, 24 column and 30 column core for each mesh model. In the calculations, all nuclides in a fuel block are distributed homogeneously in a fuel block. The same group constants were used for all calculations. The table shows that 24 meshes per block show higher k_{eff} in each core. The difference in k_{eff} between the two mesh models increases with decreasing number of fuel columns. At a 30 column core, the 24 meshes per block model shows a reactivity effect of about 0.3%Δk/k, at a 18 column core, the reactivity effect is about 0.8%Δk/k.

(2) BP reactivity

The BP reactivities at a 18 column, 24 column and 30 column core is evaluated as shown in Table 3.1.5. BP reactivities evaluated by Monte Carlo code MVP are also shown in the table. The BP reactivity in the case of the 6 mesh model is less than that of the 24 mesh model and the 24 mesh heterogeneous model. In the case of the 24 mesh heterogeneous model, the BP reactivity shows a good agreement with the reactivity effect calculated by the MVP. Errors of BP reactivity to the BP reactivity evaluated by MVP are shown in Table 3.1.6. The results of the 24 mesh heterogeneous model show good agreement with the results of the MVP code.

To check the effect of the models, BP's σ_a for f633325hl (6.3% of uranium enrichment, 33 fuel pins per block, 2.5wt% boron concentration in BP pellets, helium atmosphere and low temperature) of each model are compared in Table 3.1.7. In the thermal group, σ_as of the 24 mesh model are larger than that of the 6 mesh model because the 24 mesh model can treat the configuration of zebra type of BP using TWOTRAN-II code. Therefore, the 24 mesh model shows higher BP reactivity than the 6 mesh model.

The 24 mesh heterogeneous model shows higher BP reactivity than that of the 24 mesh model. However, most of the σ_a for the 24 mesh heterogeneous model are smaller than those of the 24 mesh model. The base case for the reactivity effects is a 24 mesh model calculation with no BP. The difference between the two models is caused by the group constants of the fuel. Group constants of the fuel for the 24 mesh heterogeneous model are produced by a harder neutron spectrum than in the case of the 24 mesh model. In the 24 mesh heterogeneous mode, a radius of fuel cell is smaller than that of the 24 mesh model. The k_{inf} of the 24 mesh heterogeneous model are small than that of the 24 mesh model as shown in Table 3.1.1 and 3.1.3. In the 24 mesh heterogeneous model, therefore, BP reactivity consists of the effects of neutron absorption by BP and the effects of the difference in the group constants of the fuel. It is considered that the fuel cell model of the 24 mesh heterogeneous model is better than that of the 24 mesh model.

(3) Effects of neutron streaming from holes

Neutron streaming through holes affects diffusion coefficients. Therefore, diffusion coefficients considering streaming effects D_{str} are evaluated by the following equation using SRAC code[9];

$$D_{str} = \frac{1}{3}\sum_{i} D_i$$

where

D_{str} : Average diffusion coefficients considering streaming effect

D_i : Diffusion coefficients in direction i considering streaming effect

Streaming effects are considered for CR guide columns, replaceable reflector blocks with coolant channels and dummy fuel blocks. The effects of each blocks are shown in Table 3.1.8. The calculations were carried out using the 24 mesh model. The streaming effects of CR guide column evaluated by Monte Carlo code MVP are also shown in the table. Streaming effects of the CR guide column are about 1%Δk/k and they are the greater part of the total streaming effects. The streaming effects become greater with decreasing number of fuel columns. The streaming effects of the dummy blocks are negligible when there are more than 18 columns in the core.

The streaming effects of CR guide columns are less than that evaluated by MVP. However, it is in fairly good agreement considering the uncertainty of Monte Carlo calculation.

(4) Effective multiplication factor during fuel loading

Effective multiplication factors (k_{eff}) during fuel loading are calculated using each model. Fig. 3.1.12 shows the change in k_{eff} during fuel loading using each model. The calculation results obtained by MVP code are also shown in Fig. 3.1.12[10]. At 30 columns, the 24 mesh model shows smaller k_{eff} than the 6 mesh model. The difference between the two models becomes small with decrease in fuel columns. It is considered that the 24 mesh model improves the BP reactivity, but in a fewer fuel columns loading, the difference looks smaller due to the mesh effect described in the above section. The 24 mesh heterogeneous model gives smaller k_{eff} than that of the 24 mesh model. It is considered that the group constants of the fuel produced by the fuel cell model with small radius give smaller k_{eff} than in the case of the 24 mesh model because each model has similar σ_a of BP.

The k_{eff} of the 24 mesh heterogeneous model with streaming correction are also shown in Fig. 3.1.12. The k_{eff} are lower about 1%Δk or more than those of the 24 mesh heterogeneous model without streaming correction. It shows good agreement with the results of Monte Carlo calculation from 24 column to 30 column. The difference at 30 column is about 0.5%Δk. Below 18 column, the difference between two models become larger.

The 24 mesh heterogeneous model shows best agreement with the Monte Carlo calculation than other models. Therefore, benchmark problems are solved using the 24 mesh heterogeneous model.

3.1.3 Results of Benchmark Problems

(1) HTTR-FC

The k_{eff} and excess reactivity ρ for the core when all control rods are fully withdrawn are shown in Table 3.1.9.

The first criticality will be achieved when 14 fuel columns are loaded. The excess reactivity at the first criticality will be 0.423%Δk/k.

(2) HTTR-CR

In HTTR, R3 control rods are fully withdrawn and the other rods are kept at the same insertion depth in operation. The control rod position means the distance from the down-side edge of fuel region. The control rod positions at criticality are shown in Table 3.1.10

(3) HTTR-EX

The k_{eff}s at 30 column, 24 column and 18 column core are shown in Table 3.1.11 where all control rods are fully withdrawn. The excess reactivity is calculated by the following equation:

$$\rho = \frac{k_{eff} - 1.0}{k_{eff}}$$

Table 3.1.1 Infinite multiplication factors obtained by DELIGHT for the 6 mesh model

Layer	ID	k_{inf}	
		Fuel cell	BP cell
1st layer	f673320hl	1.5331	1.3702
	f793320hl	1.5486	1.4012
	f943120hl	1.5876	1.4441
	f993120hl	1.5899	1.4516
2nd layer	f523325hl	1.5005	1.2980
	f633325hl	1.5255	1.3412
	f723125hl	1.5603	1.3792
	f793125hl	1.5675	1.3969
3rd layer	f433325hl	1.4702	1.2482
	f523325hl	1.5005	1.2980
	f593125hl	1.5355	1.3359
	f633125hl	1.5435	1.3490
4th & 5th layer	f343320hl	1.4174	1.1881
	f393320hl	1.4526	1.2374
	f433120hl	1.4864	1.2697
	f483120hl	1.5025	1.2992

Table 3.1.2 Infinite multiplication factors for BP cell for the 24 mesh model obtained by TWOTRAN-II

	k_{inf}	
	BP cell	Fuel cell
1st layer (2.0wt% BP)	1.3940	1.5535
2nd & 3rd layer (2.5wt% BP)	1.3302	1.5300
4th & 5th layer (2.0wt% BP)	1.2195	1.4529

Table 3.1.3 Infinite multiplication factors for fuel and BP cell for the 24 mesh heterogeneous model

Layer	ID	DELIGHT	TWOTRAN-II	
		Fuel cell	BP cell	Fuel cell
1st layer	f673320hl	1.4699	1.3866	1.5417
	f793320hl	1.4840		
	f943120hl	1.5267		
	f993120hl	1.5284		
2nd layer	f523325hl	1.4363	1.3226	1.5185
	f633325hl	1.4631		
	f723125hl	1.5011		
	f793125hl	1.5072		
3rd layer	f433325hl	1.4097		
	f523325hl	1.4363		
	f593125hl	1.4781		
	f633125hl	1.4856		
4th & 5th layer	f343320hl	1.3635	1.2204	1.4428
	f393320hl	1.3929		
	f433120hl	1.4309		
	f483120hl	1.4474		

Table 3.1.4 Mesh effect between 6 meshes per block and 24 meshes per block

Number of fuel columns	Effective multiplication factor		Mesh effect [%Δk/k]
	6 meshes per block	24 meshes per block	
30	1.2184970	1.2227019	0.2822
24	1.1889408	1.1971915	0.5797
18	1.1092833	1.1196487	0.8346

Table 3.1.5 Comparison of BP reactivity

Number of fuel columns	BP reactivity [%Δk/k]			
	6 mesh model	24 mesh model	24 mesh heterogeneous model	MVP
30	9.07	10.54	11.22	11.73
24	8.60	10.17	11.18	11.15
18	8.69	10.16	11.54	11.67

Table 3.1.6 BP reactivity error compared to Monte Carlo code MVP

Number of fuel columns	Error C/E-1* [%]		
	6 mesh model	24 mesh model	24 mesh heterogeneous model
30	-22.68	-10.14	-4.35
24	-22.87	-8.79	0.27
18	-25.54	-12.94	-1.11

* C Calculated results
E Calculated results by Monte Carlo code MVP

Table 3.1.7 Microscopic absorption cross section of ^{10}B in BP of f633325hl.

Energy Gr.	Microscopic absorption cross section [barn]		
	6 mesh model	24 mesh model	24 mesh heterogeneous model
1	5.6149×10^{-1}	5.6248×10^{-1}	5.4424×10^{-1}
2	6.5469×10^{0}	6.5274×10^{0}	6.4717×10^{0}
3	1.0188×10^{2}	1.0789×10^{2}	1.0666×10^{2}
4	3.8263×10^{2}	4.4983×10^{2}	4.7307×10^{2}
5	6.1548×10^{2}	7.0226×10^{2}	6.0342×10^{2}
6	7.8798×10^{2}	9.5068×10^{2}	8.5742×10^{2}

Table 3.1.8 Streaming effects[1)]

Number of fuel columns	Streaming effect [%Δk/k]			
	CR guide column[2)]	Upper and lower replaceable reflector[3)]	CR guide column + upper & lower reflector block[1)]	CR guide column by MVP[5)]
30	1.03	0.086	1.12	1.3
24	1.12	0.088	1.21	-
18	1.33	0.095	1.42	2.3

1) Reactivity difference between results of homogenized region and results with the diffusion coefficients considering streaming effect.
2) Streaming effects of CR guide column and irradiation column.
3) Streaming effects of upper and lower replaceable block which have coolant channels.
4) Streaming effects of CR guide column, irradiation column, upper and lower replaceable block which have coolant channels.
5) Streaming effects of CR guide column and irradiation column evaluated by Monte Carlo code MVP.

Table 3.1.9 Effective multiplication factor and excess reactivity at the first criticality.

Number of fuel columns	k_{eff}	ρ [%Δk/k]
13	0.9982249	-0.178
14	1.0042527	0.423

Table 3.1.10 Control Rod position at criticality

Number of fuel columns	Control rod position at criticality (cm)
18	264
24	187
30	153

Table 3.1.11 Effective multiplication factor and excess reactivity when 18, 24, 30 fuel columns are loaded.

Number of fuel columns	k_{eff}	Excess reactivity ρ [%Δk/k]
18	1.0381906	3.679
24	1.1229342	10.948
30	1.1610762	13.873

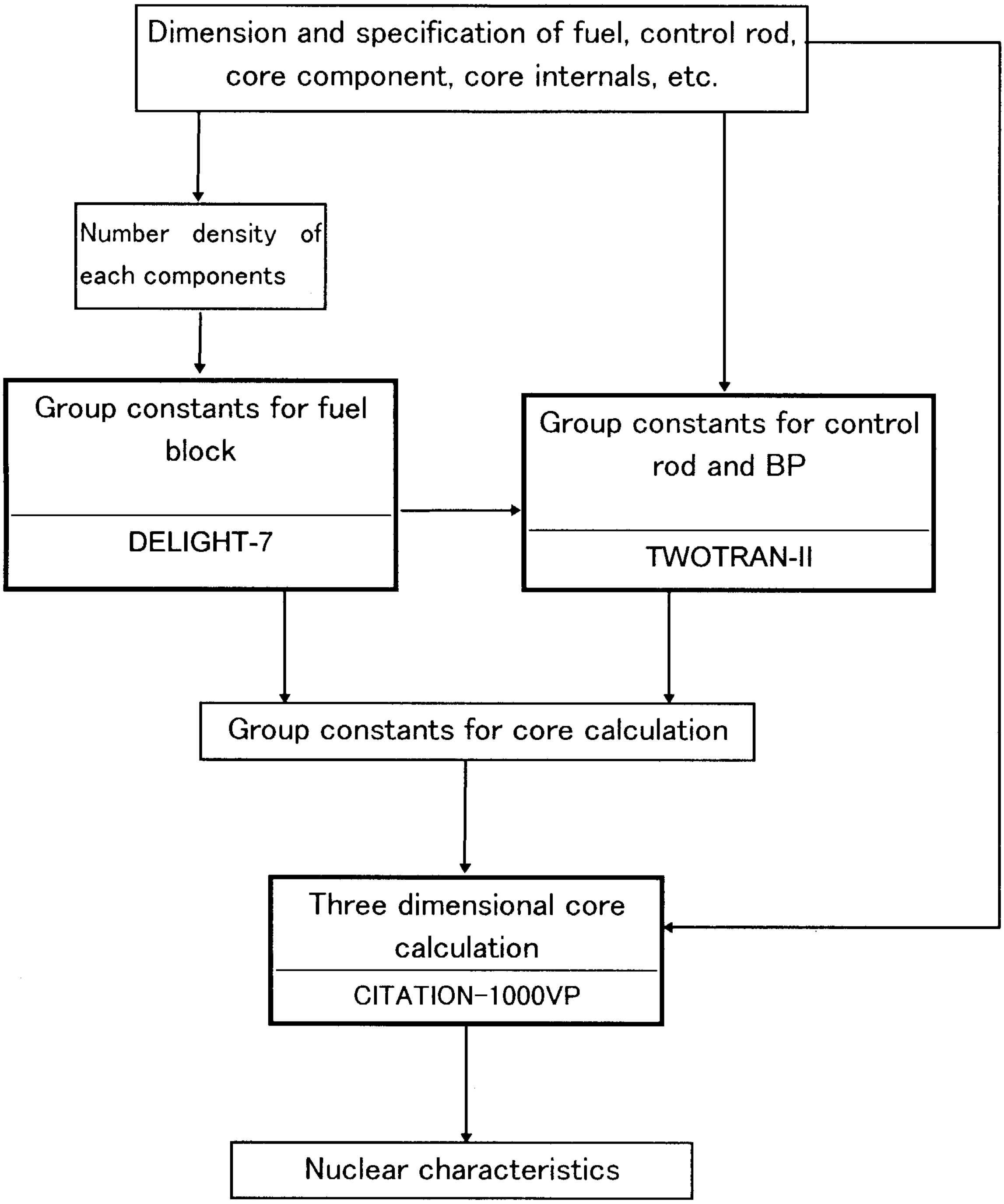

Fig. 3.1.1 Program structure of the HTTR nuclear characteristics evaluation code system

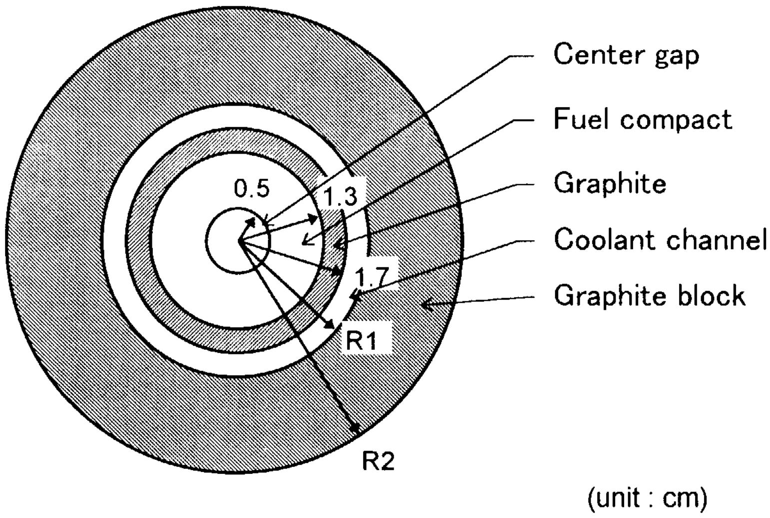

Fig 3.1.2 Fuel cell model for DELIGHT code.

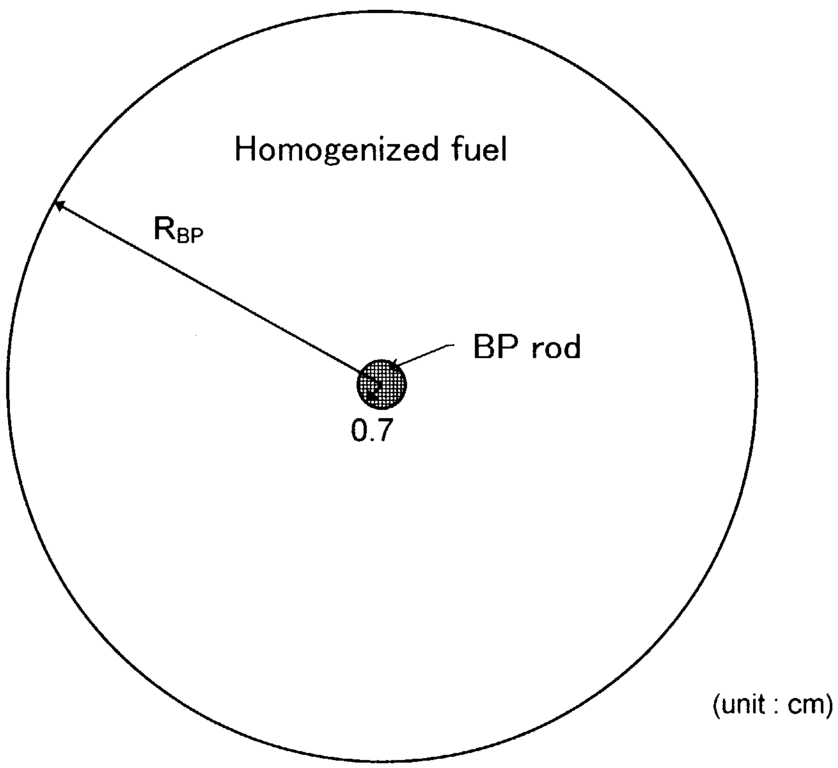

Fig. 3.1.3 BP cell model for DELIGHT code

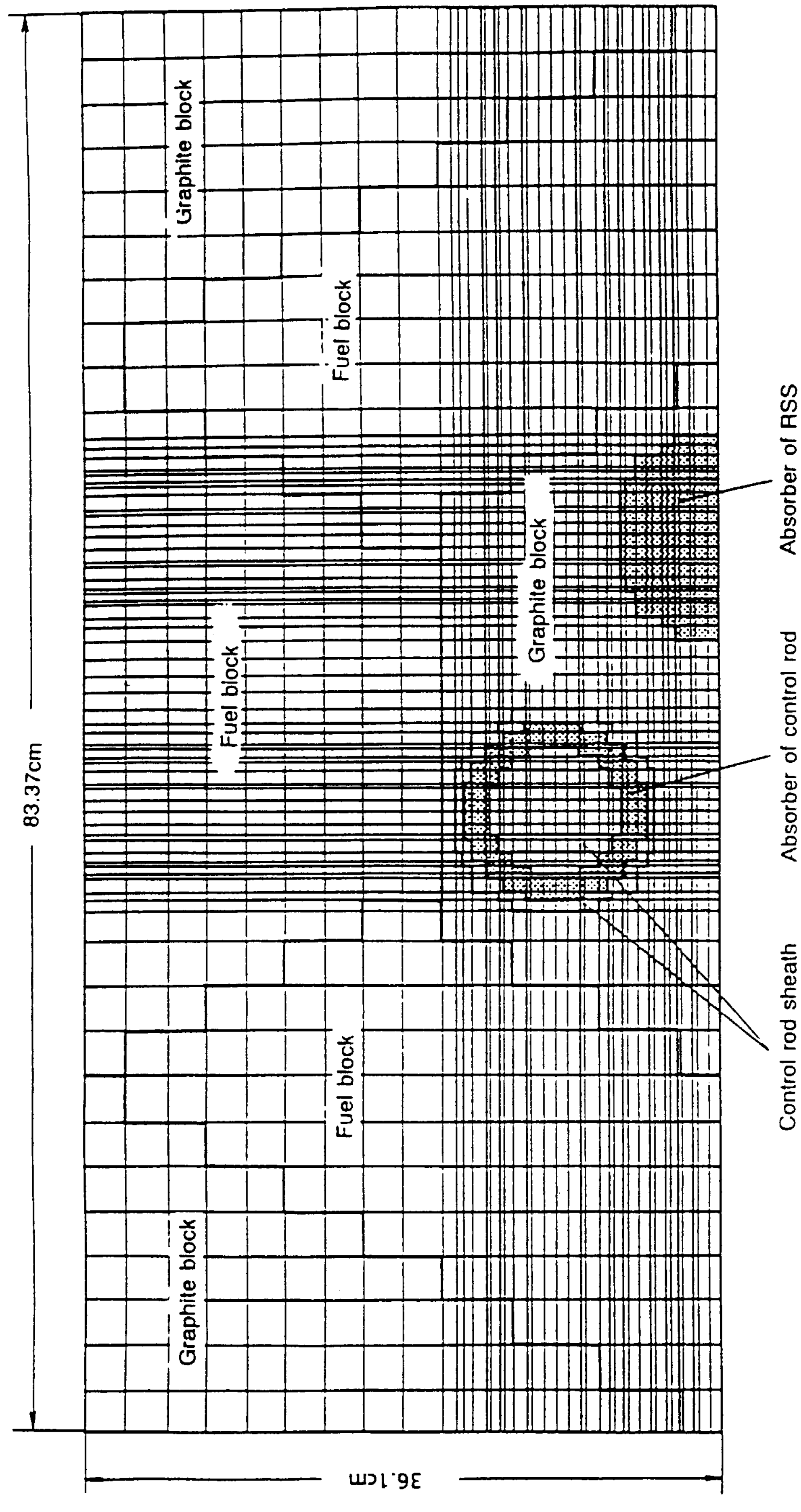

Fig. 3.1.4 Two-dimensional X-Y model of CRs for TWOTRAN-II

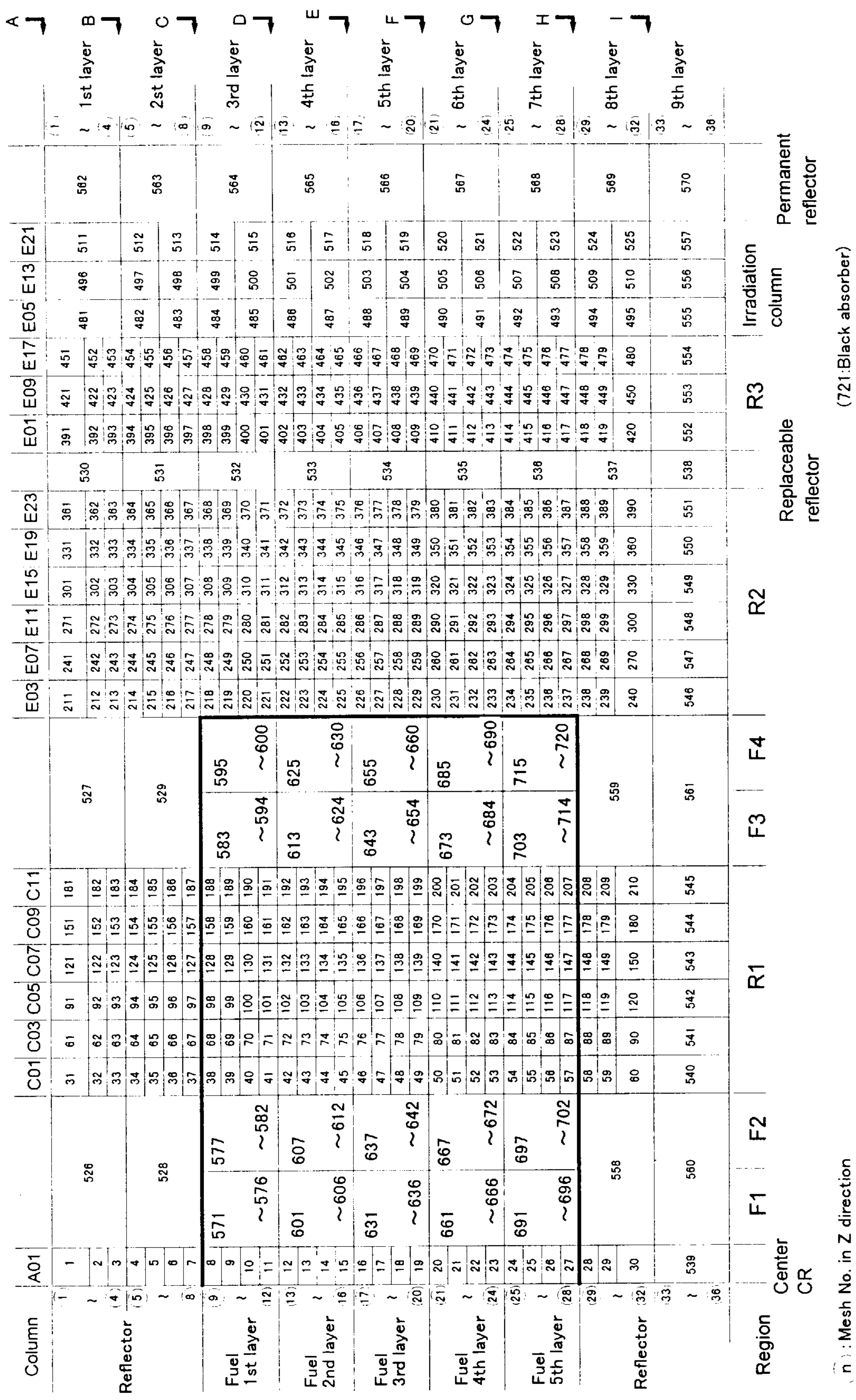

Fig. 3.1.5 r-Z plane and location of zone number for 6 mesh model

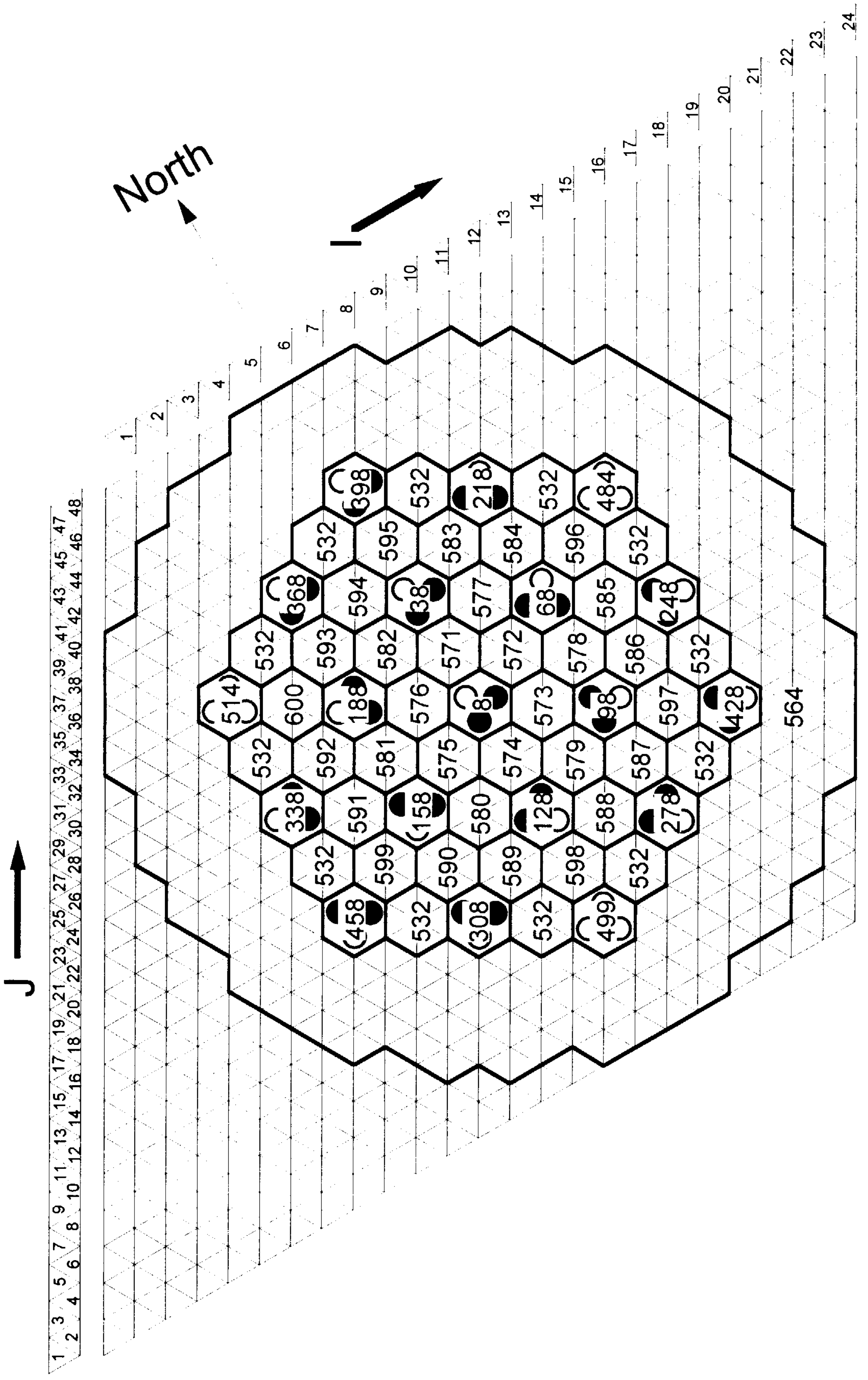

Fig. 3.1.6 Zone placement in C-C plane (3rd layer) for 6 mesh model

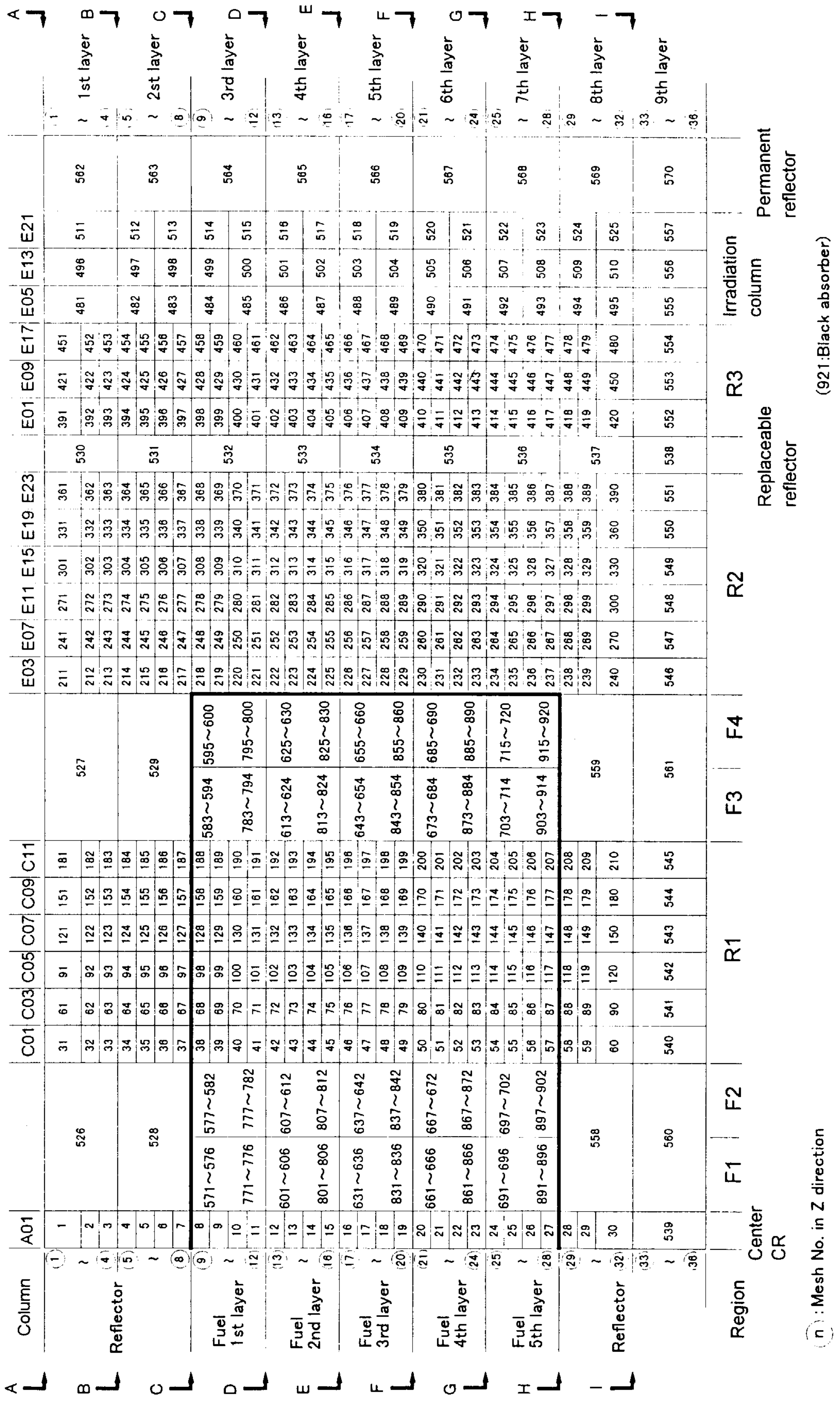

Fig. 3.1.7 r-Z plane and location of zone number for 24 mesh model

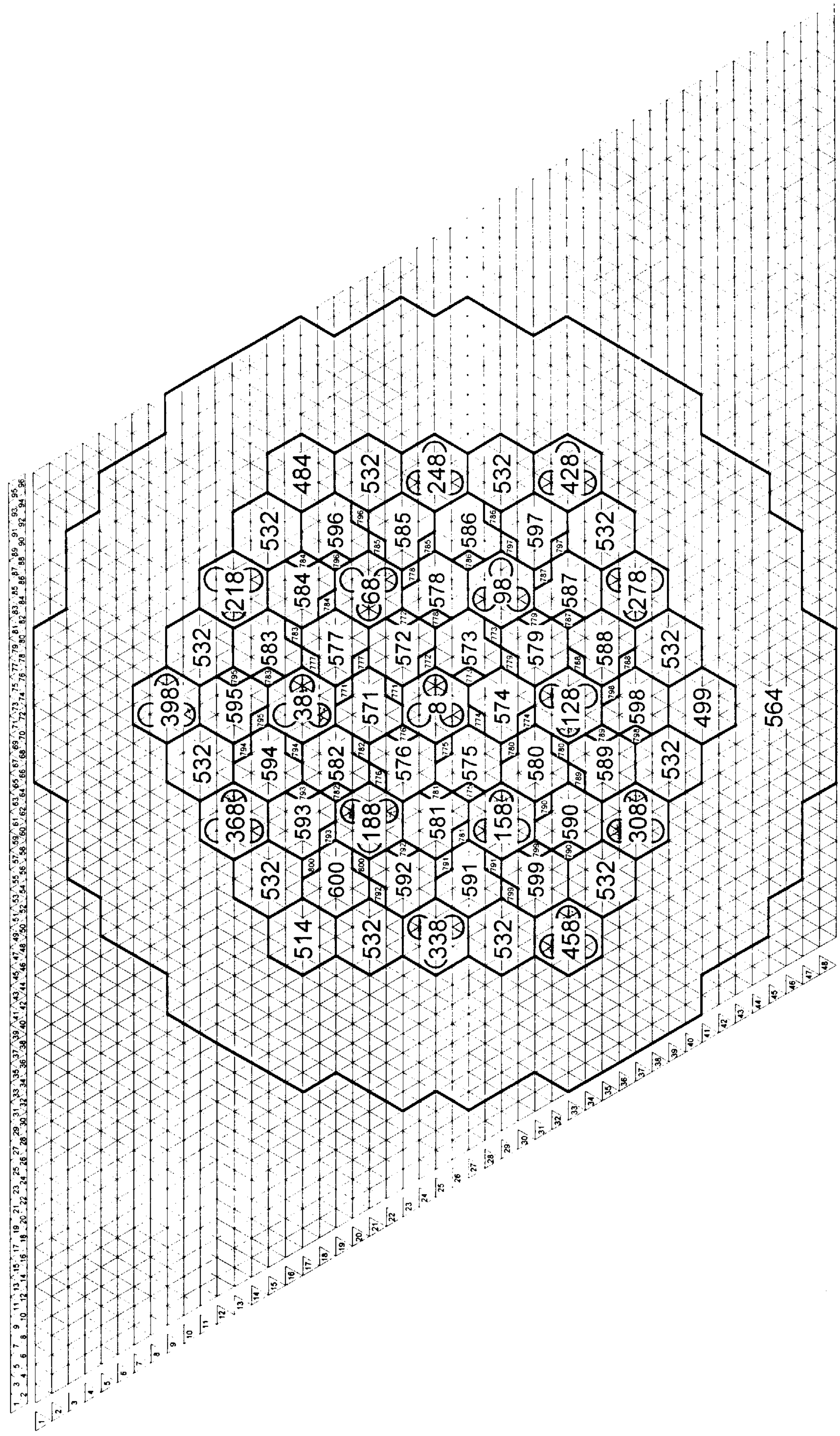

Fig. 3.1.8 Zone palcement in C-C plane (3rd layer) for 24 mesh model

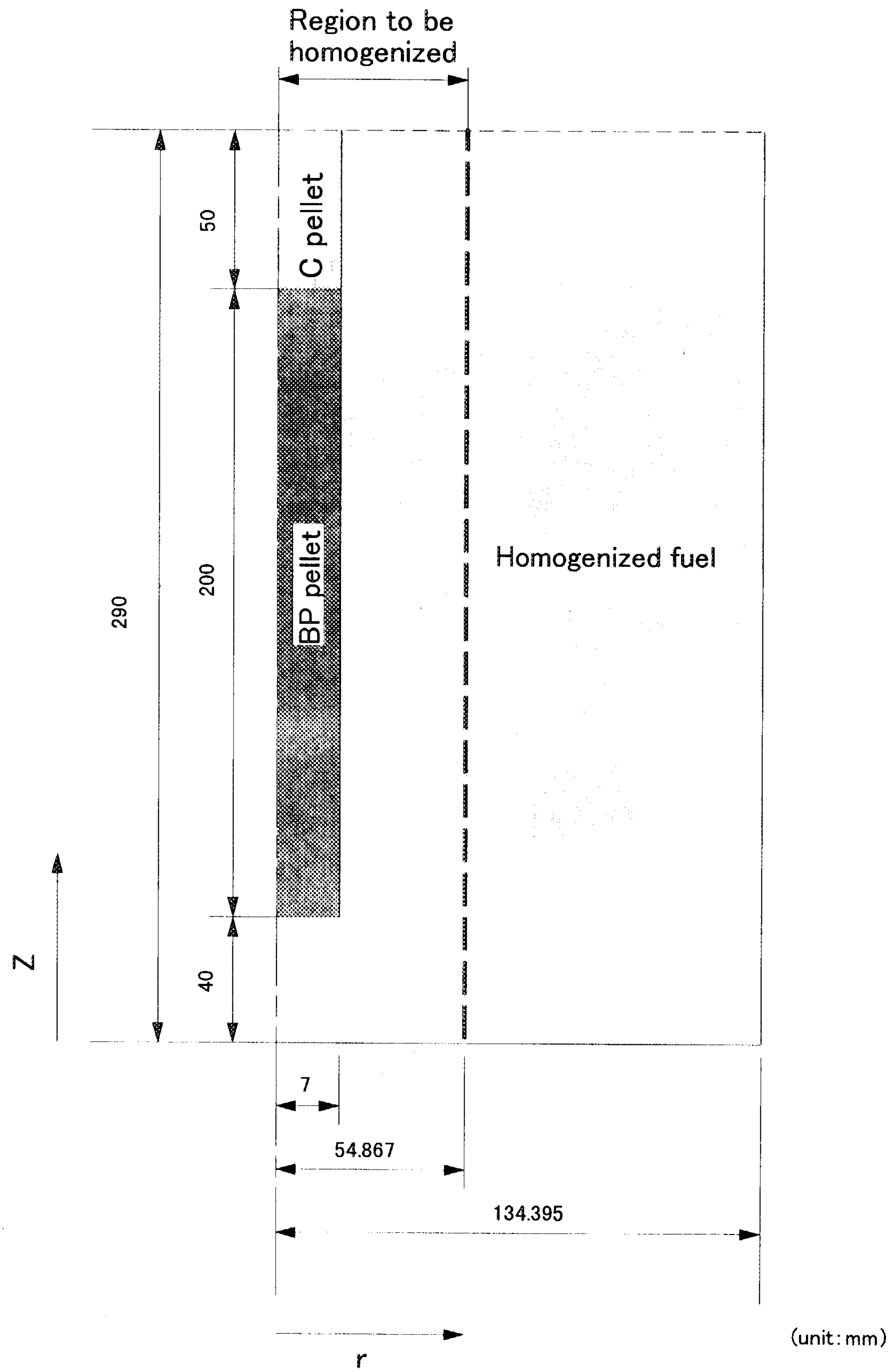

Fig. 3.1.9 BP cell configuration for 24 mesh model by TWOTRAN-II

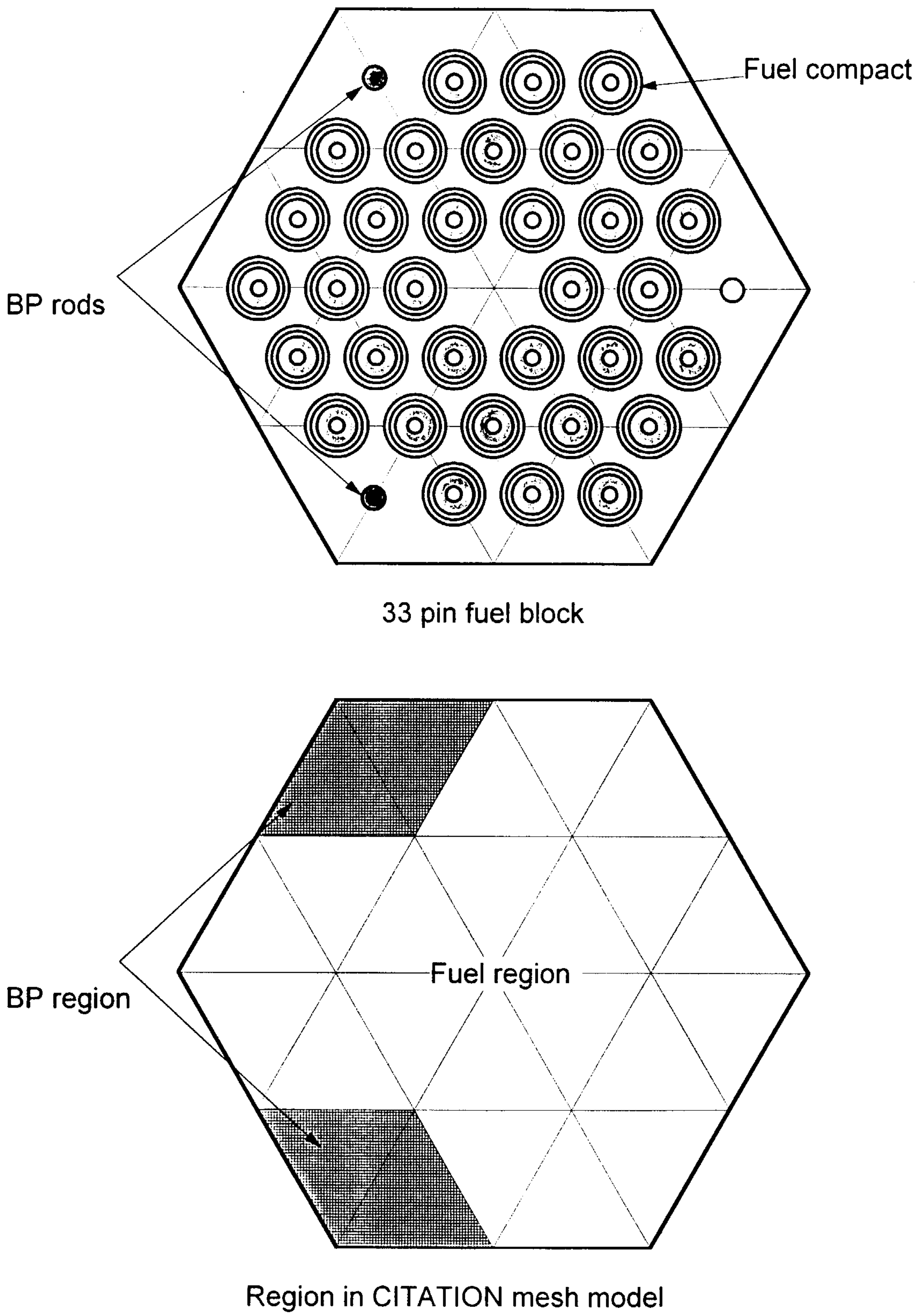

Fig. 3.1.10 Configuration of regions in block for 24 mesh heterogeneous model

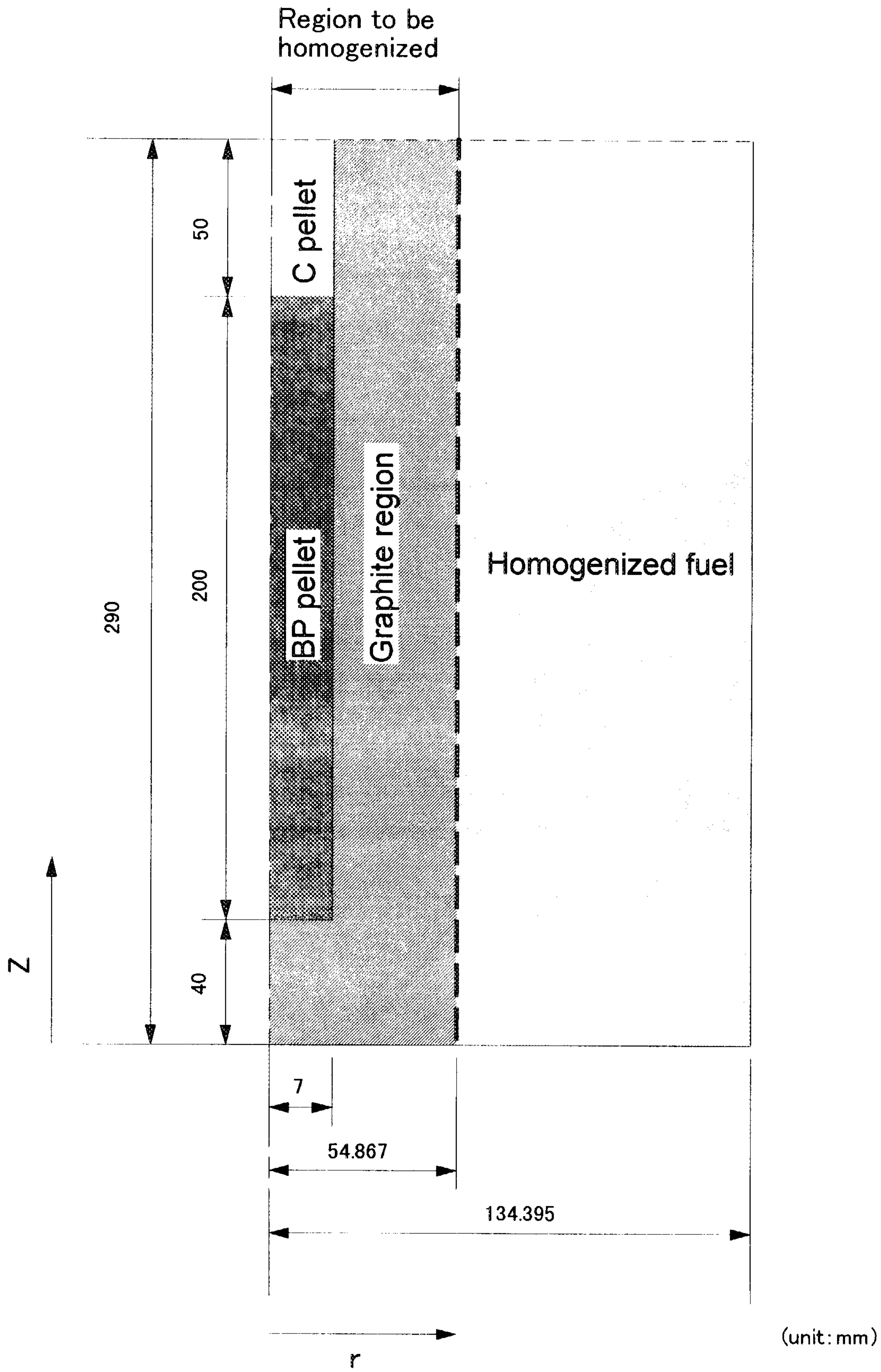

Fig. 3.1.11 BP cell configuration for 24 mesh heterogeneous model by TWOTRAN-II

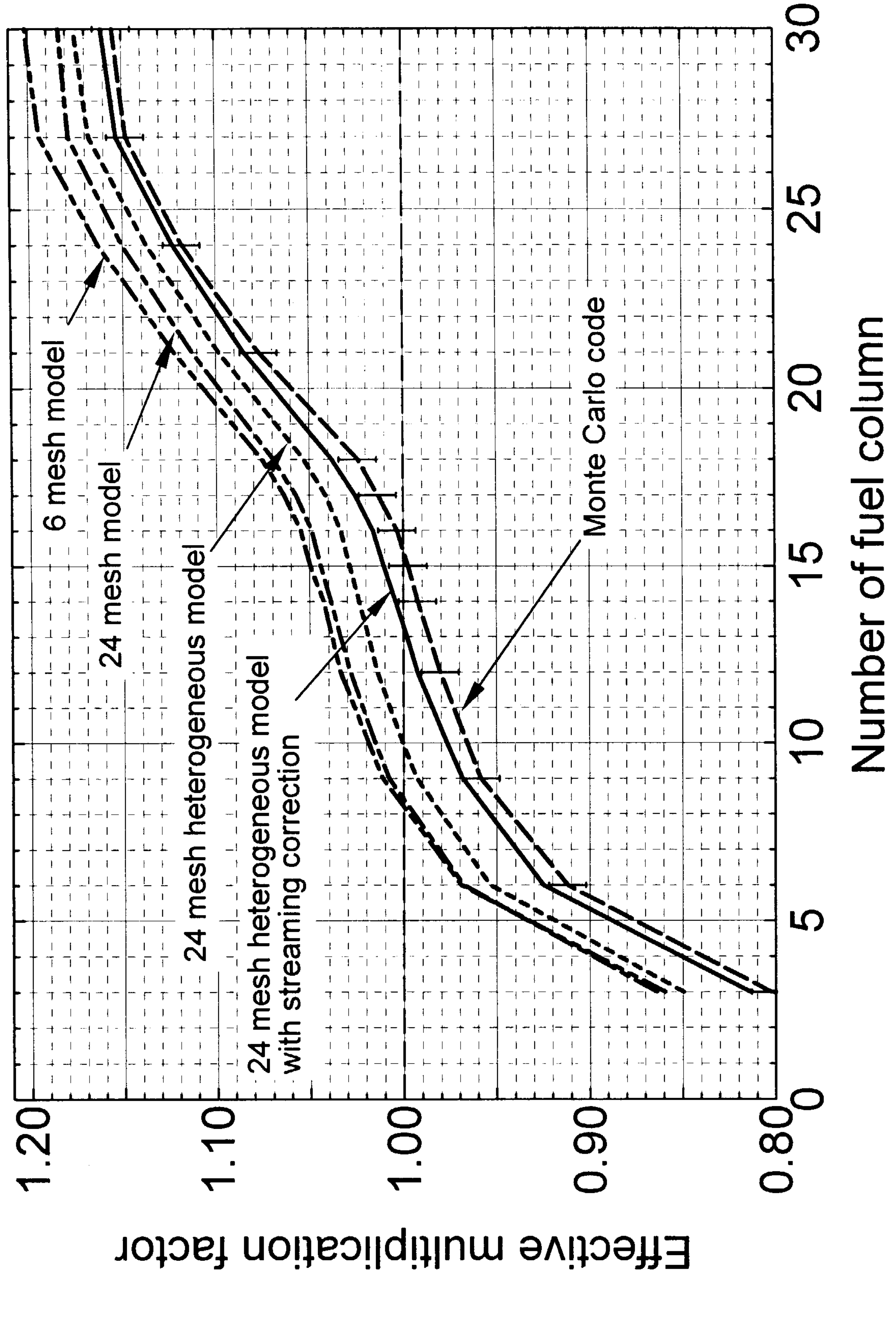

Fig. 3.1.12 Change in effective muptiplication factor during fuel loading

3.2 FZJ Diffusion Code System and Results

This chapter presents the calculational methods used in the Institute for Safety Research and Reactor Technology (ISR) of the Research Centre Jülich (FZJ) for reactor core calculations and the results for benchmark problems of the HTTR's start-up core physics experiments. Until now, two benchmark problems have been solved, the benchmark problem HTTR-FC: The number of fuel columns for the first criticality is estimated to be 16 with a small excess reactivity of 0.42%, and the benchmark problem HTTR-EX: The exess reactivity of the 18, 24, and 30 fuel column-loaded core is 2.48%, 10.27%, and 13.85%, respectively.

3.2.1 Methods and Data

An overview of the code system used in the FZJ criticality calculations is given in Fig.3.2.1.Resonance shielding is performed by the NITAWL code of the AMPX-77-system[11] applying the Nordheim integral technique to process neutron cross sections in the resonance region. The heterogeneity of the fuel compacts was taken into account by Dancoff factors which were calculated by the ZUT[12] code and supplied as input data. Cell calculations have been performed by the TOTMOS[13] program, an one-dimensional P_0 corrected transport code used for preparation of group constants as well as for one-dimensional criticality calculations.

Eigenvalues and flux distributions of the whole reactor were performed by the diffusion code CITATION[5] in triangular-z geometry. As recommended we refer to the configurations and atom densities of the materials given in the report[8].

The macroscopic absorption cross sections of the BP are affected by the neutron shielding effect. To evaluate this effect cell calculations in two-dimensional r-z geometry were performed with the transport code DORT[14].

To take into account the neutron streaming in the coolant channels as well as in the large holes in the core and the reflector, diffusion coefficient modefiers were calculated by the MARCOPOLO[15] code based on the multigroup integral transport theory. To estimate the influence of these corrections, the whole reactor calculation has been performed with and without neutron streaming correction.

All calculations refer to a 123-group cross section library[16] based on the JEF-2.2 nuclear data files.

3.2.2 Results of Analysis

(1) Dancoff Factors

As mentioned before the NITAWL code considers the heterogeneity of a system -in this case the fuel rods- by Dancoff factors. The Dancoff factor is defined as the probability that a neutron emitted isotropically from the surface of the fuel will have its next collision in other fuels surrounding the fuel element. Applying this definition to a fuel rod lattice filled with fuel in form of coated particles the ZUT code calculates the Dancoff factor as a sum of single rod Dancoff factor and the probability that a neutron leaving the first rod reaches another fuel rod and is absorbed by the fuel in that fuel rod. We calculated the Dancoff factors for all the different types of compacts by the ZUT code. These Dancoff factors are listed in Table 3.2.1 together with the corresponding U^{238} resonance integrals. On the whole, the resonance integrals increase with increasing U^{235} enrichment. The Dancoff factors remain nearly constant because they are only depending on the slightly varying geometrical conditions of the fuel compacts and rods, and the density of the graphite matrix, but not on the enrichment of the fuel.

(2) Cell Calculations

For the 15 types of BP-fuel combinations one-dimensional cell calculations in P_0 transport corrected approximation had been performed by TOTMOS using the following scheme:

1. 123 cell weighted group constants of the CFP cell model were calculated in spherical geometry using a 123 group cross section library. The cell model consists of 3 zones: the kernel, the coatings, and the corresponding matrix-zone. A white boundary condition was taken at the outer surface of the cell.
2. Then, 123 cell weighted group constants of the fuel cell were calculated in cylindrical geometry and in the same group structure as taken for the CFP cell. The zones of the cylindrical fuel cell model were: the center hole, the fuel compact, the graphite sleeve, the coolant channel, and the corresponding graphite block. The fuel cell model is shown in Fig. 3.2.2. The group constants of the materials in the fuel zone were the cell-averaged cross sections resulting from the CFP cell calculation. The cross section of the fuel cell was equivalent to the cross section of the fuel block divided by the number of fuel rods. The outer surface of the cell had a white boundary condition.
3. In the following third cell calculation the cylindrical cell model shown in Fig.3.2.3 consists of a BP rod surrounded by the second zone of homogenized fuel. The group constants of the homogenized fuel was the cell averaged 123 group constants resulting from the fuel cell

calculation. The cross section of the BP cell was the same as the cross section of the fuel block divided by the number of BP rods. At the outer cell surface an albedo of 1.0 was assumed. In this last step of cell calculations, cross sections were condensed to four broad energy groups needed for the whole reactor calculations. The energy group structure of these four groups is given in Table 3.2.2.

The k_∞-values of the CFP-, fuel- and BP-cell calculations are given in Table 3.2.3 for all 15 types of BP-fuel combinations. As it can be seen on this table the efficiency of the BP decreases with increasing U^{235} enrichment

(3) BP Adjustment

In the above result of the cell calculations, the configulation of zebra-type BP rods was not considered. A homogeneous distribution in z-direction was assumed. Due to this approximation, the axial neutron shielding effect was not taken into account.

To calculate this effect, two cases of two-dimensional cell calculations for each type of BP-fuel combination were performed with the DORT code:

1. Boron was homogenized in z-direction,
2. Heterogeneous distribution along the axis of the BP rod was taken into account.

The corresponding two-dimensional BP cell model for heterogeneous distribution used in these DORT calculations is shown in Fig. 3.2.4. As can be seen on Table 3.2.4, the difference in k_∞ of the TOTMOS and the DORT homogeneous calculation is unimportant, but the difference in the k_∞-values of the homogeneous and the heterogeneous DORT case tabulated in the last column of Table 3.2.4 is significant. In a subsequent TOTMOS calculation the B^{10} concentration was reduced in such a way that the resulting k_∞ increases about this last mentioned difference. In all BP-fuel combinations the B^{10} density had to be reduced from about 22 up to 30%.

(4) Streaming Correction

There are many holes in the core such as the insertion holes in the control rod guide blocks and of the coolant channels in the fuel and reflector blocks. The presence of these holes leads to an increased neutron streaming in the axial direction. A possibility to treat this problem within the framework of the diffusion theory is the use of anisotropic diffusion coefficients. A method for the determination of anisotropic diffusion coefficients in infinite regular cylindrical lattices is given by Benoist[15]. According to this method, the anisotropic multigroup diffusion coefficients for energy group g D^g_k (k=r,z) are calculated from the leakages of the heterogeneous lattice cells by use of the MARCOPOLO code taking into account linear anisotropic scattering. The lattice cells are subdivided into N homogeneous zones and the total cross sections together with the P_0 and P_1 group-to-group transfer cross sections in the different zones are required in the MARCOPOLO code for the calculation of the diffusion constants D^g_k (k=r,z). These cross sections were obtained as zone weighted group constants by the TOTMOS code. The anisotropic correction factors of some block assemblies are summarized in Table 3.2.5.

(5) Whole Reactor Calculations

Using the 4-energy-group cross sections from the NITAWL-TOTMOS cell calculations, the whole HTTR reactor was modelled with the CITATION diffusion code. A 3-dimensional triangular-z model was chosen. Each block was divided horizontally into 6 and vertically into 4 meshes. The horizontal cross section of the calculational model is shown in Fig. 3.2.5. The assembly was modelled by dividing the volume into spectral zones related to the material compositions. There are 45 different material zones.

Six pairs of control rods in the side reflector cannot be fully withdrawn to the top of the reflector. The effect of this CR insertion on reactivity is given as Δk=0.004 in the report[7]. In our prelimenary calculations for the first benchmark problem, we did not calculate any CR rod worth, the reactivity of Δk=0.004 was subtracted from the calculated k_{eff}-values.

According to the fuel loading scheme four series of diffusion calculations were performed:

1. All k_{eff}-values for 8 up to 30 fuel columns in the core were calculated without any streaming correction and Boron adjustment.
2. In a second series streaming corrections of the diffusion constants were considered without any BP adjustment.
3. A third series of diffusion calculations was performed under consideration of the neutron shielding effects in the BP rods, but without any streaming correction of the diffusion constants.
4. In a fourth series both corrections were taken into account: streaming corrections of the diffusion constants were considered in nearly all different spectral zones with coolant channels or holes together with the BP adjustment.

The k_{eff}-values of these four series are summarized in Tables 3.2.6 and 3.2.7 and shown in Fig.3.2.6 and 3.2.7.

The influence of the streaming correction is nearly independent of the Boron adjustment as can be recognized on these tables and the corresponding figures. With and without Boron adjustment the streaming correction causes a difference in k_{eff} from Δk=0.02 at an 8 fuel columns loading down to $\Delta k=0.015$ when there is a fully loaded core. This decrease in Δk can be explained by the fact that dummy fuel blocks with big holes and a great neutron streaming effect are subsequently replaced by fuel blocks with nearly no neutron streaming. Moreover, we found that the neutron streaming in the coolant channels of the top and bottom replaceable reflector can be neglected because the decrease in k_{eff} caused by this effect was only $\Delta k=0.0008$.

On the other hand, the neutron multiplication factors are increased by the Boron adjustment: the "Boron adjusted" k_{eff}-values are greater than the uncorrected ones, and the difference in k_{eff} increases with increasing number of fuel columns. But it is evident that the increase in the neutron multiplication factor caused by the BP adjustment is not compensated by the effec of neutron streaming.

When taking into account the neutron streaming in the channels and holes of the core and the reflector, the neutron shielding in the BP rods, and when the reactivity of the CR insertion is subtracted, the first criticality will be achieved at 16 fuel columns loading. The excess reactivity amounts to $\Delta k=0.0042$. The excess reactivity of the thin, thick, and of the fully loaded core amounts to 2.48%, 10.27%, and 13.85%, respectively.

Table 3.2.1 Dancoff Factors and U^{238} Resonance Integrals for Different Uranium Enrichments

Enr. (wt.%)	Packing Fraction (%)	Vol. of Fuel Comp. (cm^3)	Boron Impurity (ppm)	Dancoff Factor	U^{238} Res. Int.
3.301	29.6	17.63	0.95	0.7414	42.82
3.864	30.4	17.69	0.91	0.7466	43.13
4.290	30.5	17.70	0.90	0.7466	43.19
4.794	30.3	17.72	0.88	0.7478	43.21
5.162	30.5	17.65	0.90	0.7484	43.35
5.914	30.3	17.70	0.51	0.7463	43.67
6.254	29.9	17.69	0.54	0.7452	43.84
6.681	30.3	17.65	0.50	0.7461	43.91
7.189	30.8	17.69	0.85	0.7436	44.13
7.820	28.8	17.67	0.87	0.7405	43.93
9.358	29.8	17.72	0.89	0.7405	44.91
9.810	29.3	17.71	0.90	0.7423	44.90

Table 3.2.2 Few Group Strucure used in the Diffusion Calculation

Groups	Upper Energy Boundaries (eV)
1	14.92×10^6
2	1.111×10^5
3	2.902×10^1
4	1.860×10^0

Table 3.2.3 Results of the TOTMOS Cell Calculations; No Boron Adjustment

ID. No.	Enr. (wt.%)	k_∞-Values in CFP Cell	k_∞-Values in Fuel Cell	k_∞-Values in BP Cell	Δk (BP Cell-Fuel Cell)
343320	3.4	0.6282	1.4285	1.1309	-0.2977
393320	3.9	0.6562	1.4604	1.1819	-0.2785
673320	6.7	0.7782	1.5457	1.3355	-0.2102
793320	7.9	0.8208	1.5610	1.3716	-0.1894
433120	4.3	0.6771	1.4957	1.2167	-0.2790
483120	4.8	0.6995	1.5142	1.2514	-0.2627
943120	9.4	0.8713	1.5996	1.4161	-0.1835
993120	9.9	0.8854	1.6021	1.4254	-0.1766
433325	4.3	0.6771	1.4790	1.1887	-0.2903
523325	5.2	0.7163	1.5095	1.2437	-0.2658
633325	6.3	0.7619	1.5376	1.2955	-0.2421
593125	5.9	0.7484	1.5476	1.2855	-0.2621
633125	6.3	0.7619	1.5559	1.3002	-0.2557
723125	7.2	0.7969	1.5726	1.3351	-0.2375
793125	7.9	0.8208	1.5802	1.3565	-0.2237

Table 3.2.4 Infinite Multiplication Factors for the BP Cell obtained from Different Methods

ID. No.	k_∞-Values in the BP Cell				
	TOTMOS hom.	DORT hom.	Δk TOT.-DORT	DORT heterogen	Δk $DORT_{het-hom}$
343320	1.1309	1.1347	0.0038	1.1741	0.0394
393320	1.1819	1.1855	0.0036	1.2225	0.0370
673320	1.3355	1.3379	0.0023	1.3654	0.0275
793320	1.3716	1.3737	0.0021	1.3981	0.0244
433120	1.2167	1.2204	0.0037	1.2575	0.0371
483120	1.2514	1.2548	0.0034	1.2896	0.0348
943120	1.4161	1.4181	0.0020	1.4417	0.0236
993120	1.4254	1.4274	0.0019	1.4499	0.0225
433325	1.1887	1.1929	0.0041	1.2343	0.0414
523325	1.2437	1.2475	0.0037	1.2852	0.0378
63325	1.2955	1.2988	0.0033	1.3329	0.0342
593125	1.2855	1.2892	0.0037	1.3264	0.0373
633125	1.3002	1.3037	0.0036	1.3401	0.0363
723125	1.3351	1.3383	0.0032	1.3719	0.0335
793125	1.3565	1.3594	0.0029	1.3908	0.0313

Table 3.2.5 Streaming Correction Factors obtained by the MARCOPOLO Code

Group	Streaming Correction Factors for the					
	CR Guide Block CB-1		CR Guide Block CB-3		Rep.Ref.Block RB-1	
	D_r/D_{hom}	D_z/D_{hom}	D_r/D_{hom}	D_z/D_{hom}	D_r/D_{hom}	D_z/D_{hom}
1	1.1403	1.5740	1.1562	1.6317	1.0199	1.0513
2	1.1761	1.9333	1.1963	2.0358	1.0246	1.0786
3	1.1812	1.9497	1.2016	2.0537	1.0286	1.0836
4	1.1877	2.0243	1.2090	2.1369	1.0307	1.0908

Table 3.2.6: k_{eff}-Values for Different Fuel Columns Loading
Reactivity Effect for CR Insertion considered (Δk=0.004)
with BP Adjustment

Core Region	No. of Fuel Col.	No Stream.Corr. BP Adjustm.	Δk	Stream.Corr. BP Adjustm.
F3+F4	8	0.9700	-0.0208	0.9492
	9	0.9802	-0.0206	0.9596
	10	0.9880	-0.0204	0.9676
	11	0.9961	-0.0200	0.9761
	12	1.0024	-0.0197	0.9827
	13	1.0072	-0.0195	0.9877
	14	1.0128	-0.0192	0.9936
	15	1.0180	-0.0189	0.9991
	16	1.0229	-0.0187	1.0042
	17	1.0313	-0.0184	1.0129
	18	1.0434	-0.0180	1.0254
+F2	19	1.0616	-0.0177	1.0439
	20	1.0768	-0.0174	1.0594
	21	1.0902	-0.0171	1.0731
	22	1.1058	-0.0169	1.0889
	23	1.1187	-0.0163	1.1024
	24	1.1317	-0.0167	1.1145
+F1	25	1.1429	-0.0164	1.1265
	26	1.1532	-0.0162	1.1370
	27	1.1628	-0.0159	1.1469
	28	1.1677	-0.0157	1.1520
	29	1.1721	-0.0155	1.1566
	30	1.1760	-0.0153	1.1607

Table 3.2.7 k_{eff}-Values for Different Fuel Columns Loading
Reactivity Effect for CR Insertion considered (Δk=0.004)
No BP Adjustment

Core Region	No. of Fuel Col.	No Stream.Corr. No BP Adjustm.	Δk	Stream.Corr. No BP Adjustm.
F3+F4	8	0.9513	-0.0205	0.9308
	9	0.9613	-0.0203	0.9410
	10	0.9688	-0.0200	0.9488
	11	0.9767	-0.0197	0.9570
	12	0.9828	-0.0194	0.9634
	13	0.9875	-0.0193	0.9683
	14	0.9930	-0.0190	0.9740
	15	0.9980	-0.0187	0.9793
	16	1.0028	-0.0185	0.9843
	17	1.0110	-0.0181	0.9928
	18	1.0227	-0.0176	1.0051
+F2	19	1.0403	-0.0175	1.0228
	20	1.0550	-0.0172	1.0378
	21	1.0679	-0.0169	1.0510
	22	1.0830	-0.0169	1.0662
	23	1.0960	-0.0167	1.0793
	24	1.1075	-0.0166	1.0910
+F1	25	1.1187	-0.0163	1.1023
	26	1.1285	-0.0161	1.1123
	27	1.1376	-0.0159	1.1217
	28	1.1421	-0.0157	1.1265
	29	1.1461	-0.0154	1.1307
	30	1.1497	-0.0153	1.1344

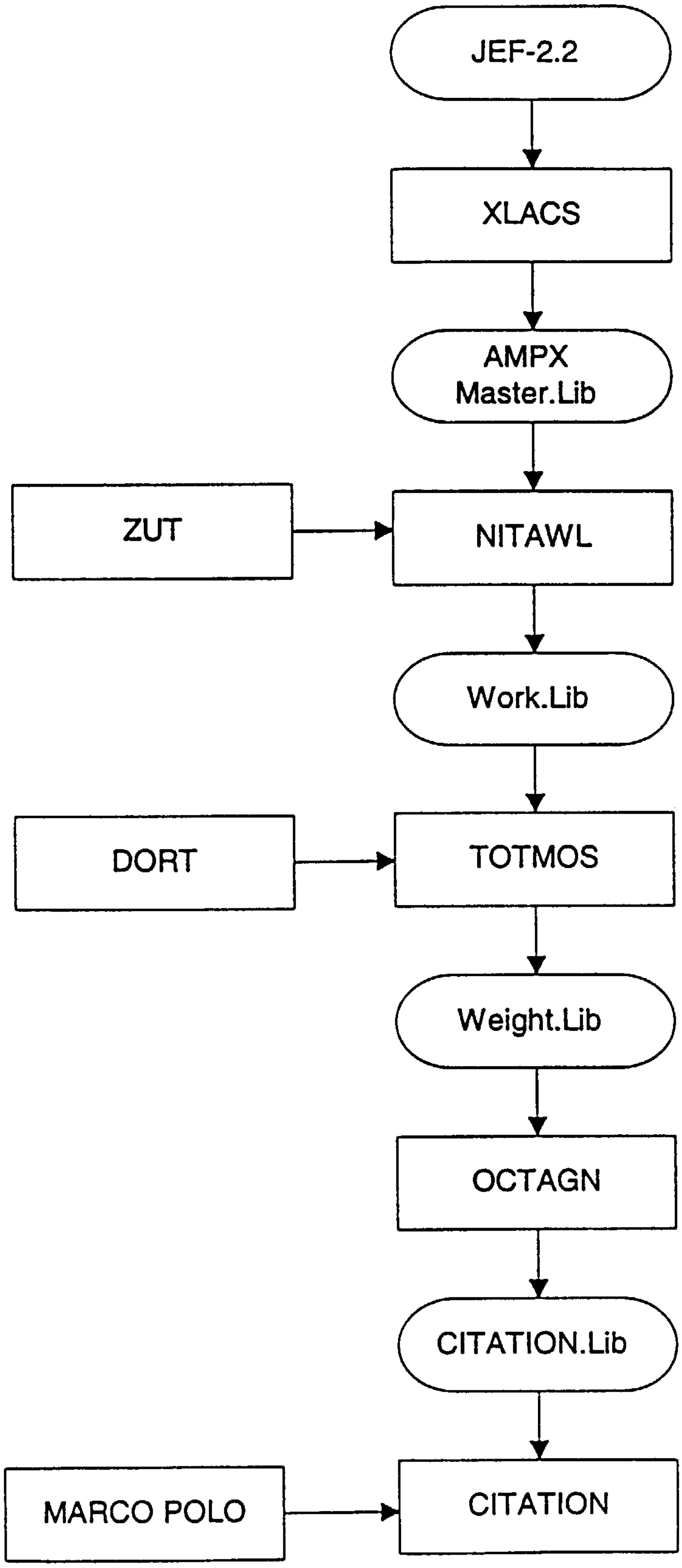

Fig. 3.2.1 Overview of the TOTOMOS-CITATION code system

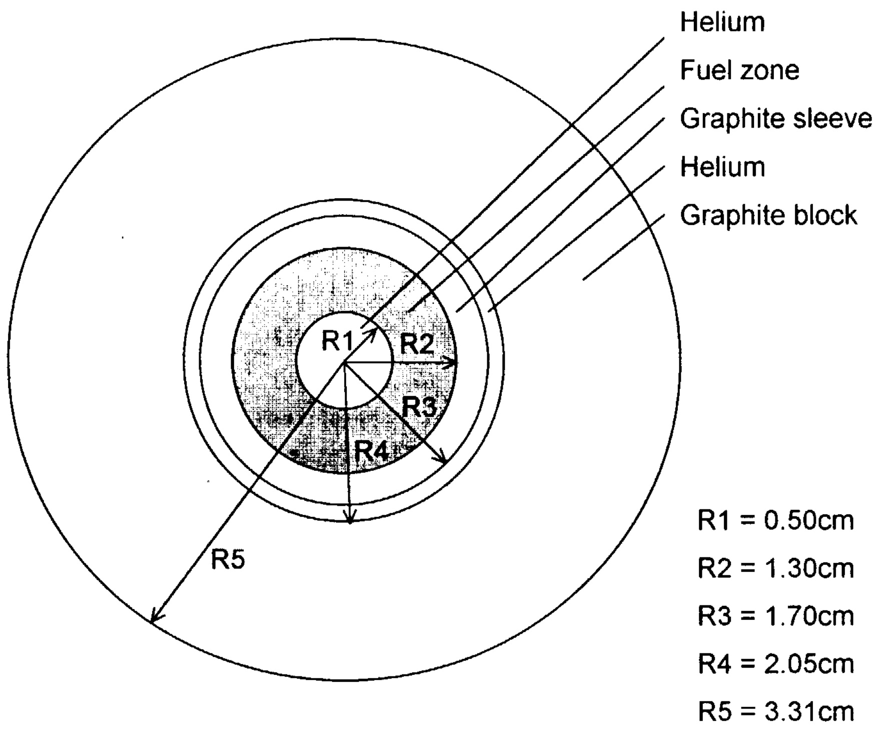

Fig. 3.2.2 1-d cylindrical fuel cell model for TOTOMOS

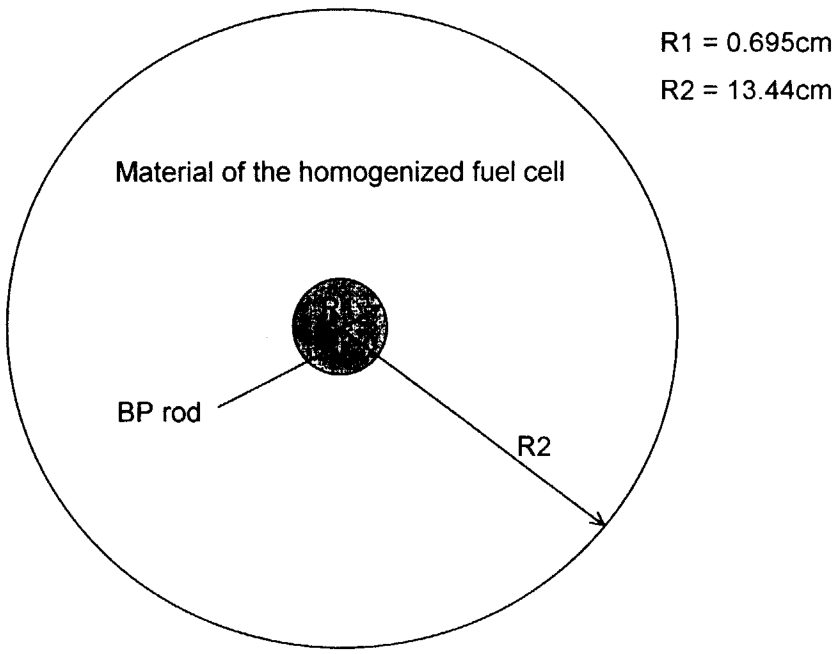

Fig. 3.2.3 1-d cylindrical BP cell model for TOTOMOS

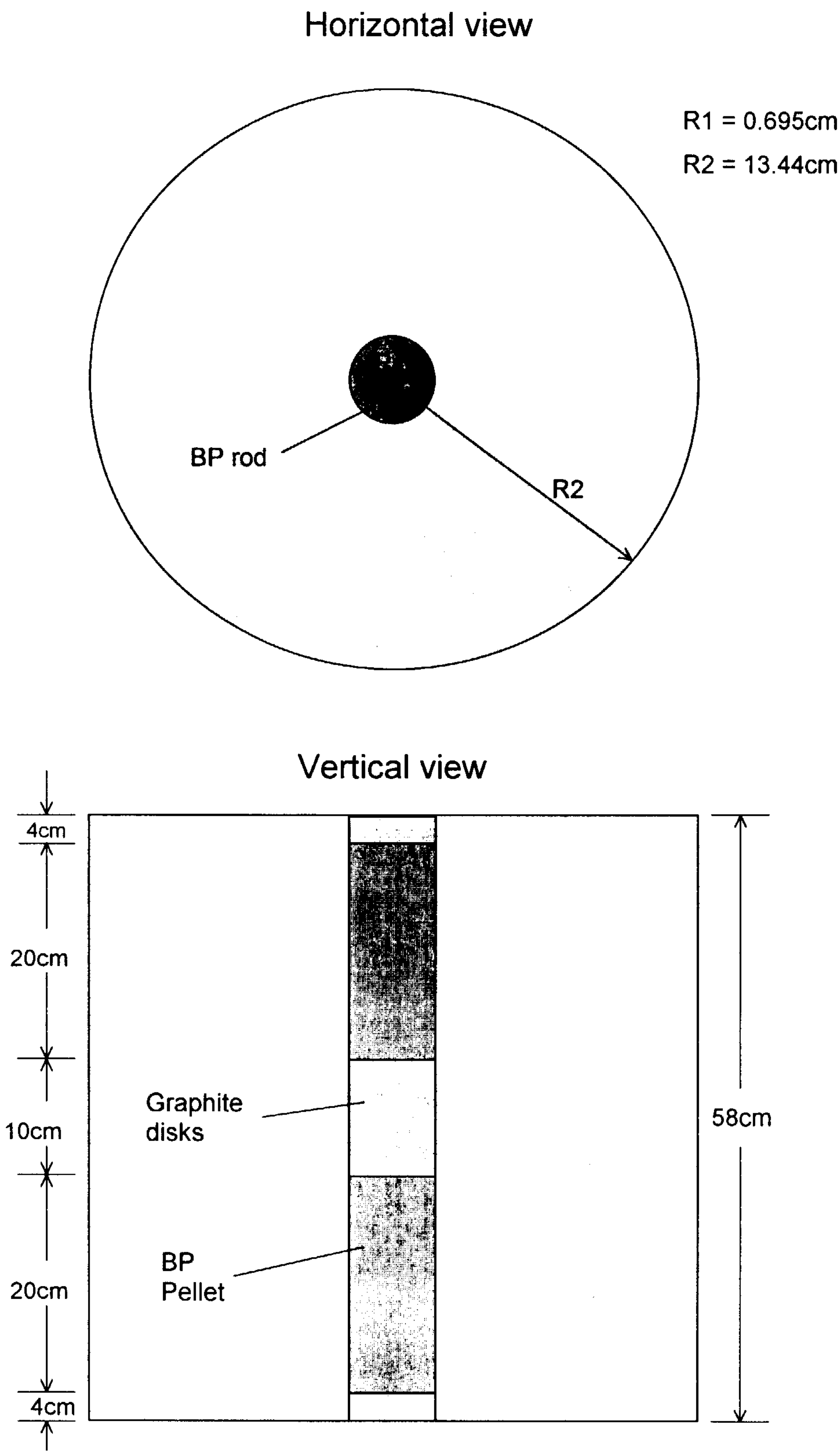

Fig. 3.2.4 2-d cylindrical BP cell model for DORT

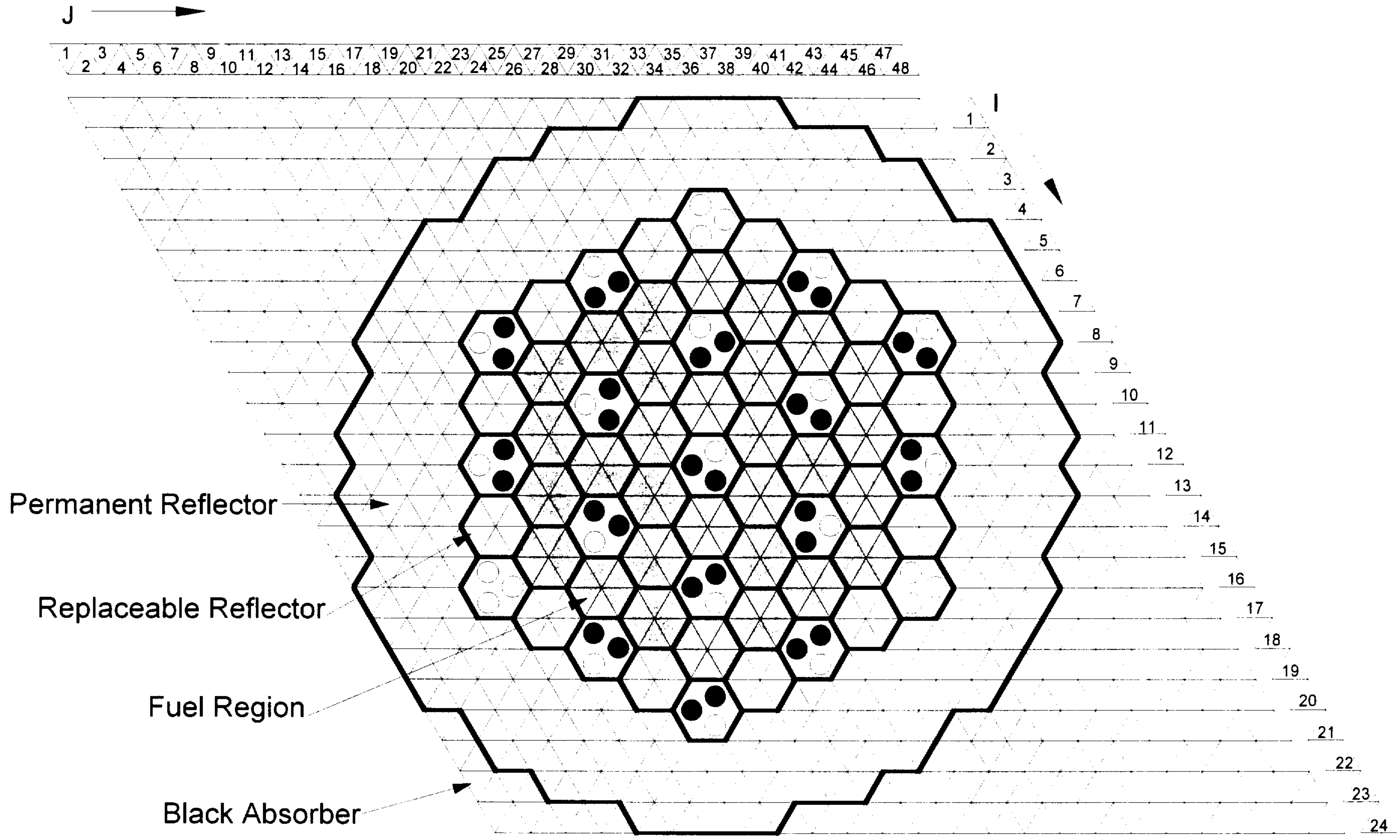

Fig. 3.2.5 Horizontal Cross Section of the Core Model

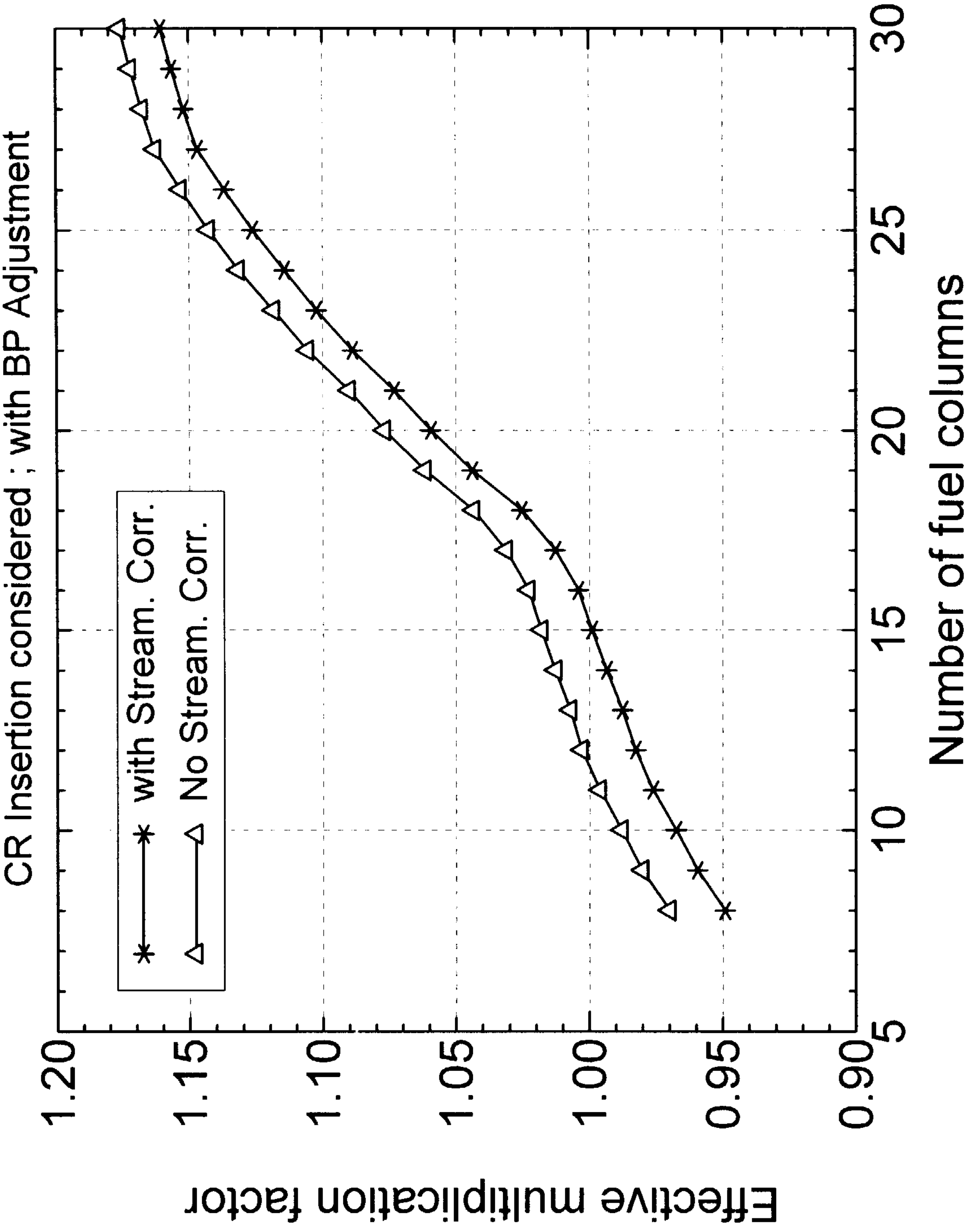

Fig.3.2.6 : k_{eff}–Values for Different Fuel Columns in the Core

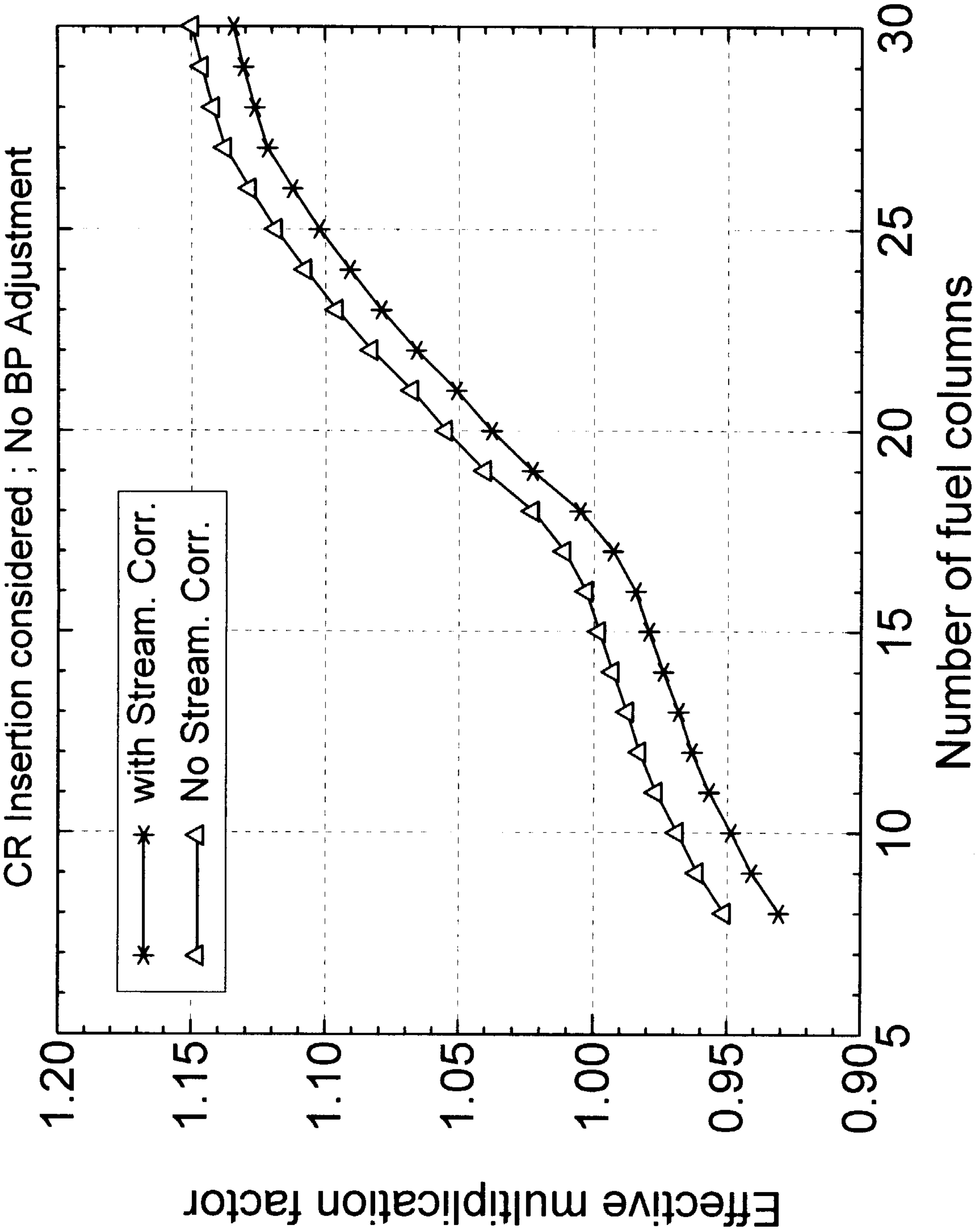

Fig.3.2.7 : k_{eff}–Values for Different Fuel Columns in the Core

4. Comparison and Analysis of the Results

4.1 Comparison of the Results Obtained by each Code System

The results obtained with the HTTR 24 mesh heterogeneous model and FZJ diffusion code systems are shown in Table 4.1.1 and Fig. 4.1.1 together with the results from the HTTR Monte Carlo calculation[10]. Compared to the Monte Carlo results, it is obvious that the two diffusion calculations overestimate k_{eff}, but the HTTR results show an overestimation of more than 1% in the region of the 12 to 18 fuel column-loaded core, whereas the FZJ values show nearly no deviation to the MVP results in the same region of core loading. The diffusion calculations were performed in both cases by the CITATION code, the cell calculations were carried out by the DELIGHT and TWOTRAN codes on the part of HTTR, and by the TOTMOS and DORT codes on the part of FZJ.

The group constants for these whole reactor calculations were taken from those BP cell calculations whose k_∞-values are summarized in Table 4.1.2 together with the corresponding BP efficiencies. In the case of the HTTR cell calculations, the group constants for the BP region in all fuel blocks of one layer were taken from one cell calculation, because the microscopic B^{10} absorption cross sections for the different fuel blocks in one layer did not differ strongly. In the FZJ calculation each fuel block was considered. As can be seen in this table, the corresponding BP efficiences are not so different. But when regarding the corresponding microscopic ^{10}B absorption cross sections shown in Table 4.1.3 and 4.1.4, large differences can be noticed in the thermal groups. These large discrepancies in the basic thermal ^{10}B absorption cross section may be one reason for the different k_{eff}-curves of HTTR and FZJ. But in the HTTR calculations the Boron absorption cross sections are only valid in the BP region of a fuel block in this 24mesh heterogeneous model, whereas in the FZJ calculations the B^{10} group constants are effective cross sections for the whole fuel block.

4.2 Analysis of the Discrepancies in the HTTR and FZJ Results

Although the calculated HTTR k_{eff}-values are conservative from a safety point, the reason for this large discrepancy to the HTTR Monte Carlo and FZJ diffusion calculations should be somewhat clearer. Therefore, several items which could contribute to this discrepancy were examined.

At first, the streaming effects were compared. As can be seen on Table 4.2.1, the difference between both streaming effects are not important, but the FZJ calculations show a higher streaming effect, especially in the case of only few fuel column-loaded core.

Secondly, a small study in the influence of the few group structure on k_{eff} was carried out. A simple whole core model for the CITATION calculation was assumed: the core was totally filled (37 fuel columns) with one fuel block type f633325 (with 6.3wt.% Uranium enrichment, 33 fuel pins per block, and a 2.5 wt.% Boron concentration in the BP pellets) and surrounded by one replaceable reflector block type A-1 1/3[11]. As can be seen on Table 4.2.2 the increase from the four group structure with one thermal group to the six group structure with three thermal groups causes only a small, but positive reactivity effect on k_{eff}. Like the streaming effect, it contributes only a minor part to the discrepancy, but it is not the main reason.

Third: As the greatest differences exist between the HTTR and FZJ results using both the "6 mesh model": the calculation results are shown in Table 4.2.3 with no streaming correction and with 6 horizontal meshes in the whole core calculations.

In order to have a common basis , the HTTR calculations considering the self-shielding of the BP by a "big" radius of the BP cell have to be compared with the FZJ calculations considering the BP self-shielding by Boron adjustment. In both cases, BP self-shieldng is taken into account, but the methods differ significantly. The infinite multiplication factors of each fuel and BP cell obtained by these two methods are summarized on Table 4.2.4 together with the corresponding BP efficiencies. As can be seen on this table, the BP efficiency decreases in both cases from the inner to the outer side of a fuel layer, and it increases with increasing fuel layer number. The differencies in the BP efficiency of both methods have the same tendencies: they decrease when going to the outer core region and increase versus the bottom of the core. But it is obvious that in all fuel block types, the TOTMOS BP cell calculations with their adjusted ^{10}B densities show higher BP efficiencies than the DELIGHT cell calculations with the higher BP cell radius and the high ^{10}B concentration in the inner zone of the BP cell.

Therefore, the influence of these different BP self-shielding methods on the whole core calculations was analysed in a small study. We assumed the simplified whole core model mentioned above, in order to eliminate all minor and disturbing effects: we chose only one fuel block type as fuel and one reflector block type as reflector as it was already done in the comparison of the group structure. The test calculations consisted of two steps:

- a BP-fuel cell calculation for the fuel block type 633325 and a cell calculation for one replaceable reflector type (A-1 1/3) were executed by the TOTMOS code. Cell weighted condensation was performed to six broad energy groups. In the HTTR cell calculation using the 6 mesh model, the self-shielding of the Boron in the BP rod was taken into account by increasing the radius of the BP cell about the factor of $\sqrt{(58/40)}$, but taking in the BP zone itself the high concentration of the B_4C as it exists in the pellets. On the other hand, the radius of the BP cell in the FZJ calculations was not changed. Instead of this, the ^{10}B densities were adjusted in the one-dimensional TOTMOS cell calculations in such a way that the resulting k_∞-values were the same as those yielding from the corresponding two-dimensional DORT calculations considering the heterogeneous distribution of the BP in the BP rod (see Fig.3.2.4 of chapter 3.2).

- Using the group constants of these cell calculations, a whole core calculation was done with the above mentioned simplified core model: a triangular-z model with 6 meshes horizontally and 4 meshes vertically and with only two material zones: a fuel zone and a surrounding reflector zone as described above. The reflector zone itself was surrounded by a black absorber and the front and back boundary conditions were reflected ones. In this whole core model no CR guide blocks or dummy fuel blocks were taken into account.

Two series of cell calculations were performed:

- one with a BP cell radius of r=16.20 cm and the high Boron concentration in the inner zone of the BP cell,
- and another one with a BP cell radius of r=13.44cm, and the B^{10} adjusted density taken over the total length of the fuel block in the inner zone of the BP cell.

The results of these BP cell calculations obtained by the TOTMOS code are summarized in Talbe 4.2.5 together with the BP efficiencies. The difference in the BP efficiency is 1.41% $\Delta k/k$. The macroscopic ^{10}B absorption cross sections are listed in Table 4.2.6 together with the correspondig k_{eff}-values obtained by the CITATION calculation. The k_{eff}-values obtained by CITATION calculations without Boron in the BP rods are included into this table together with the corresponding BP efficiencies. One can recognize that the thermal cross section of the "small" cell is higher about 12 to 13% than that of the "big" cell. The two different methods of self-shielding cause a difference of 1.41% $\Delta k/k$ in the cell calculation, but only a difference of 0.47% $\Delta k/k$ in the corresponding simplified whole core calculation.

All discrepancies yielded by the test calculations and given by the slightly different streaming effects are listed in Table 4.2.7. When summing up all effects, only a difference of 0.75% $\Delta k/k$ can be explained. But in the case of the fully loaded core with which these test calculations can be compared a little a discrepancy of 1.80% $\Delta k/k$ exists between the two different diffusion calculations. Thus, the aberrations found by this analysis are not sufficient to explain a remaining difference of about 1% $\Delta k/k$. Moreover, the results of HTTR 24 mesh heterogeneous model shows good agreement with the results of FZJ code system at 30 column but the difference between both code system becomes large with decreaseing the number of fuel column. Therefore, it is proposed to perform calculations with and without BP for thin and thick annular core, as well as for fully loaded core in order to determine more exactly the BP efficiencies in the whole core.

Table 4.1.1: Comparison of k_{eff}-Values obtained from Different Calculational Methods

CR Insertion is considered

Calculational Method	HTTR Diffusion Calculation		FZJ Diffusion Calculation		Monte Carlo Calculation
No. of Fuel Col.	24 mesh het. model with Streaming Corr.		6 mesh model with Streaming Corr. with BP Adjustment		HTTR (MVP)
	k_{eff}	%Δk/k (to MVP)	k_{eff}	%Δk/k (to MVP)	k_{eff}
6	0.9251	1.55	0.9182	0.74	0.9120
9	0.9684	1.07	0.9596	0.12	0.9585
12	0.9926	1.25	0.9827	0.24	0.9804
14	1.0162	1.18	0.9936	0.11	0.9925
15	1.0043	1.28	0.9991	0.15	0.9976
16	1.0105	1.26	1.0042	0.08	1.0034
17	1.0257	1.16	1.0129	-0.07	1.0136
18	1.0382	1.31	1.0254	0.10	1.0243
21	1.0850	0.68	1.0731	-0.35	1.0771
24	1.1229	0.39	1.1145	-0.28	1.1180
27	1.1533	0.39	1.1469	-0.09	1.1481
30	1.1611	0.43	1.1607	0.40	1.1553

Table 4.1.2: Comparison of BP-Efficiencies in the Different Cell Calculations

Fuel Layer	ID of Fuel Block	FZJ TOTMOS			HTTR TWOTRAN-II*		
		k_∞ Fuel Cell	k_∞ BP Cell	BP-Eff. (%Δk/k)	k_∞ Fuel Cell	k_∞ BP Cell	BP-Eff. (%Δk/k)
1st Layer	f673320	1.5457	1.3630	8.67	1.5417	1.3866	7.26
	f793320	1.5610	1.3960	7.57			
	f943120	1.5996	1.4397	6.94			
	f993120	1.6021	1.4480	6.64			
2nd Layer	f523325	1.5095	1.2815	11.79	1.5185	1.3226	9.75
	f633325	1.5376	1.3297	10.17			
	f723125	1.5726	1.3686	9.48			
	f793125	1.5802	1.3878	8.77			
3rd Layer	f433325	1.4790	1.2301	13.68			
	f523325	1.5095	1.2815	11.79			
	f593125	1.5476	1.3227	10.98			
	f633125	1.5559	1.3365	10.55			
4th& 5th Layer	f343320	1.4285	1.1703	15.45	1.4428	1.2204	12.63
	f393320	1.4604	1.2189	13.57			
	f433120	1.4957	1.2538	12.90			
	f483120	1.5142	1.2862	11.71			

* The BP cell calculations of HTTR refer to the 24 mesh heterogeneous model and yield group constants only for the BP region of the fuel block (see Fig. 3.1.6 of chapter 3.1). The group constants for the fuel region of the fuel blocks are calculated by a DELIGHT fuel cell calculation with r_{cell}= 3.11 or 3.21cm.

Table 4.1.3: Microscopic B^{10} Absorption Cross Sections Obtained by HTTR TWOTRAN-II Calculation

ID of Fuel Block	σ_{abs} (barn) of ^{10}B		
	f393320	f633325	f793320
Group			
1	5.445×10^{-1}	5.442×10^{-1}	5.444×10^{-1}
2	$6.480\times10^{+0}$	$6.472\times10^{+0}$	$6.475\times10^{+0}$
3	$1.090\times10^{+2}$	$1.067\times10^{+2}$	$1.075\times10^{+2}$
4	$5.059\times10^{+2}$	$4.731\times10^{+2}$	$5.033\times10^{+2}$
5	$6.979\times10^{+2}$	$6.034\times10^{+2}$	$6.591\times10^{+2}$
6	$1.024\times10^{+3}$	$8.574\times10^{+2}$	$9.998\times10^{+2}$

Table 4.1.4: Microscopic B^{10} Absorption Cross Sections obtained by FZJ TOTMOS Calculation

ID of Fuel Block	σ_{abs} (barn) of ^{10}B		
	f393320	f633325	f793320
Group			
1	7.341×10^{-1}	7.337×10^{-1}	7.344×10^{-1}
2	$2.539\times10^{+1}$	$2.522\times10^{+1}$	$2.521\times10^{+1}$
3	$2.243\times10^{+2}$	$2.207\times10^{+2}$	$2.231\times10^{+2}$
4	$1.261\times10^{+3}$	$1.086\times10^{+3}$	$1.131\times10^{+3}$

Table 4.2.1: Comparison of Streaming Effects

Number of Fuel Columns	Streaming Effect (%$\Delta k/k$)		
	HTTR	FZJ	Difference
18	1.42	1.68	0.26
24	1.21	1.36	0.15
30	1.12	1.12	0.0

Table 4.2.2 Influence of the Number of Broad Groups on k_{eff}

Groups	k_{eff}	%Δk/k
4	1.20164	
6	1.20568	0.28

Table 4.2.3 Comparison of k_{eff}-Values obtained by HTTR and FZJ Diffusion Calculation

No. of Fuel Col.	k_{eff} 6 mesh model no Streaming Corr. with BP Self-Shielding CR Insertion considered		Difference Δk	Difference %Δk/k
	HTTR	FZJ		
9	1.0113	0.9802	0.0311	3.14
12	1.0336	1.0024	0.0312	3.01
14	1.0427	1.0128	0.0299	2.83
15	1.0497	1.0180	0.0317	2.97
16	1.0547	1.0229	0.0318	2.95
17	1.0637	1.0313	0.0324	2.95
18	1.0756	1.0434	0.0322	2.87
21	1.1226	1.0902	0.0324	2.65
24	1.1634	1.1317	0.0317	2.41
27	1.1942	1.1628	0.0314	2.26
29	1.1994	1.1721	0.0273	1.94
30	1.2014	1.1760	0.0253	1.80

Table 4.2.4 k_∞-Values and the Corresponding BP-Efficiencies of the Different Cell Models

Fuel Layer	ID of Fuel Block	TOTMOS			DELIGHT			Diff. in BP-Eff.
		k_∞		BP-Eff. (%Δk/k)	k_∞		BP-Eff. (%Δk/k)	
		Fuel Cell	BP Cell		Fuel Cell	BP Cell		
1st Layer	f673320	1.5457	1.3630	8.67	1.5331	1.3702	7.75	0.92
	f793320	1.5610	1.3960	7.57	1.5486	1.4012	6.79	0.78
	f943120	1.5996	1.4397	6.94	1.5876	1.4441	6.26	0.68
	f993120	1.6021	1.4480	6.64	1.5899	1.4516	5.99	0.65
2nd Layer	f523325	1.5095	1.2815	11.79	1.5005	1.2980	10.40	1.39
	f633325	1.5376	1.3297	10.17	1.5255	1.3412	9.01	1.16
	f723125	1.5726	1.3686	9.48	1.5603	1.3792	8.42	1.06
	f793125	1.5802	1.3878	8.77	1.5675	1.3969	7.79	0.98
3rd Layer	f433325	1.4790	1.2301	13.68	1.4702	1.2482	12.10	1.58
	f523325	1.5095	1.2815	11.79	1.5005	1.2980	10.40	1.39
	f593125	1.5476	1.3227	10.98	1.5355	1.3359	9.73	1.25
	f633125	1.5559	1.3365	10.55	1.5435	1.3490	9.34	1.21
4th Layer	f343320	1.4285	1.1703	15.45	1.4174	1.1881	13.62	1.83
	f393320	1.4604	1.2189	13.57	1.4526	1.2374	11.97	1.60
	f433120	1.4957	1.2538	12.90	1.4864	1.2697	11.48	1.42
	f483120	1.5142	1.2862	11.71	1.5025	1.2992	10.41	1.30

Table 4.2.5 Infinite Multiplication Factors Obtained by Different Cell Models for the Fuel Block f633325

$r_{BP\text{-}Cell}$ (cm)	13.44	16.20
$N^{10}{}_{B}$ (at/(b cm)) in BP Rod	2.7845-4	5.6049-4
k_∞ of Fuel Cell	1.5376	1.5376
k_∞ of BP Cell	1.3297	1.3550
BP-Efficiency (%Δk/k)	10.17	8.76

Table 4.2.6 k_{eff}-Values of the Whole Core Test Calculations and the Corresponding Macroscopic ^{10}B Cross Sections

$r_{BP\ Cell}$ (cm)	13.44	16.20
Group	Σ_{abs} of B^{10} (cm^{-1})	
1	4.403×10^{-7}	6.008×10^{-7}
2	4.952×10^{-6}	6.748×10^{-6}
3	8.258×10^{-5}	1.071×10^{-4}
4	3.519×10^{-4}	4.231×10^{-4}
5	6.896×10^{-4}	6.876×10^{-4}
6	1.036×10^{-3}	9.135×10^{-4}
k_{eff} with B in BP	1.2356	1.2427
k_{eff} no B in BP	1.42125	1.42111
BP-Efficiency %Δk/k	10.57	10.10

Table 4.2.7 Reactivity Increase Caused by Different Calculational Methods in the Test Cases

Item	Reactivity Effect (%Δk/k)
Group Effect 4→6	0.28
Different BP-Shielding Effect	0.47
Sum	0.75

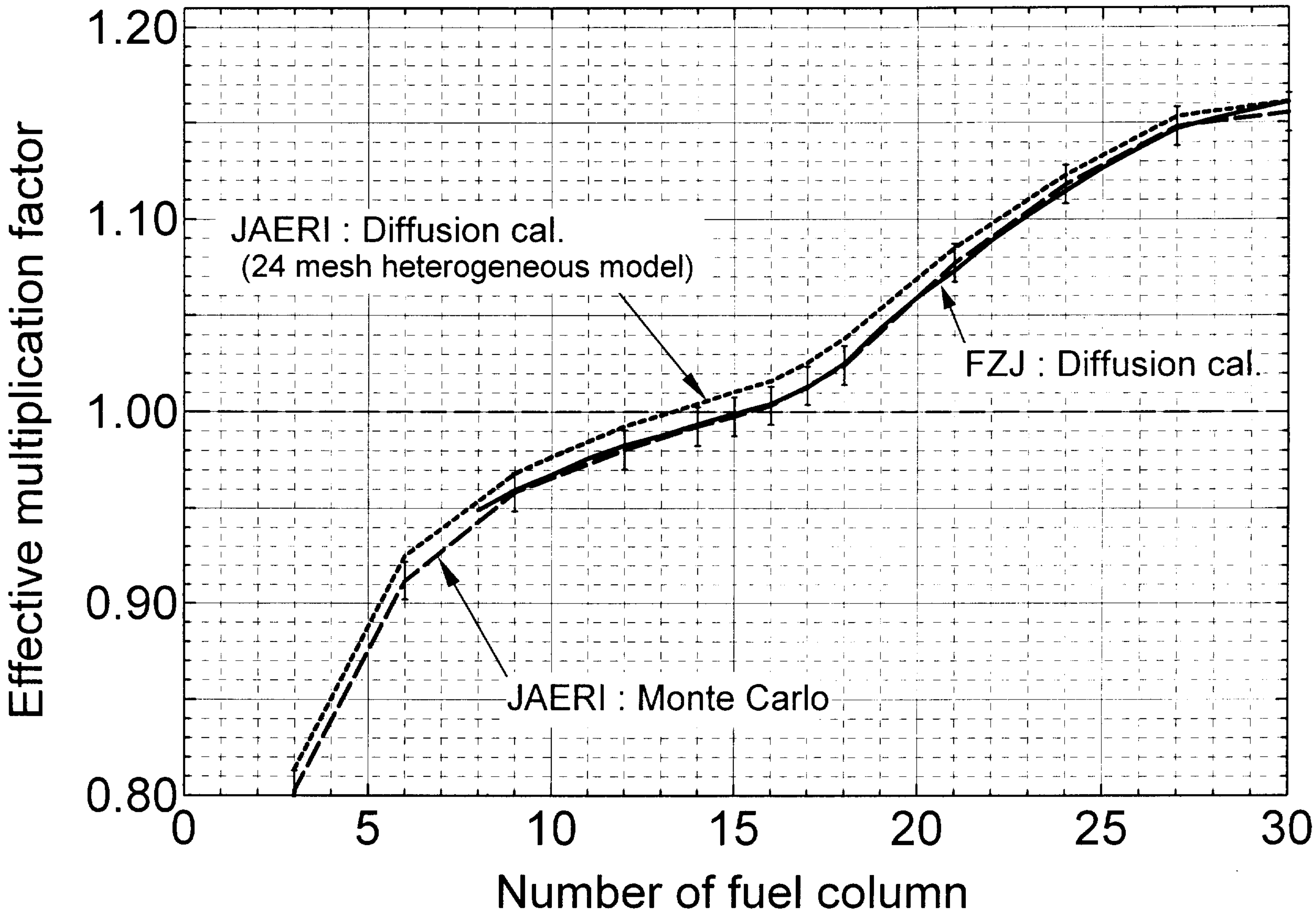

Fig 4.1.1 Change in effective multiplication factor during fuel loading

5. Conclusion

The calculation models and results of JAERI and FZJ for HTTR Benchmark problems are compared. As the results, the effects of energy group number, streaming effect became clear. For the FZJ code system, sensitivity analyses for BP cell were conducted.

In both calculational methods improvements can be proposed. In the case of the HTTR diffusion calculations, calculation model for annluar core and fewer columns core should be improved because descripancy between the results of Monte Carlo calculation becomes larger with decreasing the number of fuel column.

In the FZJ calculation the reactivity of Boron may be overestimated to some extent, the self-shielding effect of Boron in radial direction has to be considered . Furthermore, the asymmetrical position of the BP rods and the greater C region around the BP rods in the edges of the hexagonal fuel block should be taken into account.

In both calculational methods the effective radius of the BP cell and the corresponding atomic densities of the Boron have to be optimized. This is necessary to obtain more exact results concerning the BP efficiency in the whole core.

Acknowledgments

The authors express their sincere thanks to N. Nojiri, T. Tanaka, W. Scherer, H. Ando, and H. Mogi for their useful comments and support.

References

1) K. Yamashita et. al., "Nuclear design of the High-Temperature Engineering Test Reactor (HTTR)", Nucl. Sci. Eng. 122,212-228 (1996).

2) R. Shindo, K. Yamashita and I. Muarta, "DELIGHT-7; One-dimensional fuel cell burnup analysis code for High Temperature Gas-cooled Reactors (HTGRs)", JAERI-M 90-048, (1990)(in Japanese).

3) K. D. Lathrop and F. W. Brinkley, "TWOTRAN-II : and interfaced exportable version of the TWOTRAN code for two-dimensional transport", LA-4848-MS, (1973).

4) H. Harada and K. Yamashita, "The reactor core analysis code CITATION-1000VP for High Temperature Engineering Test Reactor", JAERI-M 89-135 (1989)(in Japanese).

5) T. B. Fowler, D. R. Vondy and G. W. Cunningham, "Nuclear reactor core analysis code, CITATION", ORNL-TM-2496 (1971).

6) T. Mori and M. Nakagawa, "MVP/GMVP : General purpose Monte Carlo codes for neutron and photon transport calculations based on continuous energy and multigroup methods", JAERI-Data/Code 94-007 (1994)(in Japanese).

7) N. Nojiri et al., "Evaluation of Accuracy of Monte Carlo Code MVP with VHTRC Experiments -Multiplication Factor at Criticality, Burnable Poison Worth and Void Worth-", JAERI-Trch 97-060 (1997)(in Japanese).

8) N. Nojiri et al., Private communication.

9) K. Okumura, K. Kaneko and K. Tsuchihashi, "SRAC95 ; General purpose neutronics code system", JAERI-Data /Code 96-015 (1996)(in Japanese).

10) N. Nojiri et al., "Preliminary Analyses for HTTR's Start-up Physics Tests by Monte Carlo Code MVP", JAERI-Tech 98-03 (1998)(in Japanese).

11) N.M.Greene et al.,"AMPX-77:A Modular Code System for Generating Coupled Multigroup Neutron-Gamma Cross Section Libraries from ENDF/B-IV and/or ENDF/B-V", ORNL/CSD/TM-238 (1992)

12) E. Teuchert, K.A. Haas, "ZUT-DGL-VSOP: Progrmmzyklus für die Resonanzabsorption in heterogenen Anordnungen", FZ-Jülich, Interner Bericht IRE-70-1 (1970)

13) H. Brockmann, "TOTMOS: An Integral Transport Code for Spectrum Calculations", FZ-Jülich, ISR (1995)

14) W.A. Rhoades et al.,"DORT-TORT, Two- and Three-Dimensional Discrete Ordinates Transport, Version 5.13.14", ORNL CCC-543 (1992)

15) CH. Yang and P. Benoist, Nucl. Sci. Eng., 86, 47-62 (1984)

16) P. Phlippen, Private Communication (1997).

国際単位系 (SI) と換算表

表 1　SI 基本単位および補助単位

量	名　称	記　号
長　さ	メートル	m
質　量	キログラム	kg
時　間	秒	s
電　流	アンペア	A
熱力学温度	ケルビン	K
物質量	モル	mol
光　度	カンデラ	cd
平面角	ラジアン	rad
立体角	ステラジアン	sr

表 2　SI と併用される単位

名　称	記　号
分，時，日	min, h, d
度，分，秒	°, ′, ″
リットル	l, L
トン	t
電子ボルト	eV
原子質量単位	u

$1\ \mathrm{eV} = 1.60218 \times 10^{-19}\ \mathrm{J}$

$1\ \mathrm{u} = 1.66054 \times 10^{-27}\ \mathrm{kg}$

表 5　SI 接頭語

倍数	接頭語	記　号
10^{18}	エクサ	E
10^{15}	ペタ	P
10^{12}	テラ	T
10^{9}	ギガ	G
10^{6}	メガ	M
10^{3}	キロ	k
10^{2}	ヘクト	h
10^{1}	デカ	da
10^{-1}	デシ	d
10^{-2}	センチ	c
10^{-3}	ミリ	m
10^{-6}	マイクロ	μ
10^{-9}	ナノ	n
10^{-12}	ピコ	p
10^{-15}	フェムト	f
10^{-18}	アト	a

表 3　固有の名称をもつ SI 組立単位

量	名　称	記号	他の SI 単位による表現
周波数	ヘルツ	Hz	s^{-1}
力	ニュートン	N	$m \cdot kg/s^2$
圧力，応力	パスカル	Pa	N/m^2
エネルギー，仕事，熱量	ジュール	J	N·m
工率，放射束	ワット	W	J/s
電気量，電荷	クーロン	C	A·s
電位，電圧，起電力	ボルト	V	W/A
静電容量	ファラド	F	C/V
電気抵抗	オーム	Ω	V/A
コンダクタンス	ジーメンス	S	A/V
磁束	ウェーバ	Wb	V·s
磁束密度	テスラ	T	Wb/m^2
インダクタンス	ヘンリー	H	Wb/A
セルシウス温度	セルシウス度	℃	
光束	ルーメン	lm	cd·sr
照度	ルクス	lx	lm/m^2
放射能	ベクレル	Bq	s^{-1}
吸収線量	グレイ	Gy	J/kg
線量当量	シーベルト	Sv	J/kg

表 4　SI と共に暫定的に維持される単位

名　称	記　号
オングストローム	Å
バーン	b
バール	bar
ガル	Gal
キュリー	Ci
レントゲン	R
ラド	rad
レム	rem

$1\ \mathrm{Å} = 0.1\ \mathrm{nm} = 10^{-10}\ \mathrm{m}$

$1\ \mathrm{b} = 100\ \mathrm{fm^2} = 10^{-28}\ \mathrm{m^2}$

$1\ \mathrm{bar} = 0.1\ \mathrm{MPa} = 10^5\ \mathrm{Pa}$

$1\ \mathrm{Gal} = 1\ \mathrm{cm/s^2} = 10^{-2}\ \mathrm{m/s^2}$

$1\ \mathrm{Ci} = 3.7 \times 10^{10}\ \mathrm{Bq}$

$1\ \mathrm{R} = 2.58 \times 10^{-4}\ \mathrm{C/kg}$

$1\ \mathrm{rad} = 1\ \mathrm{cGy} = 10^{-2}\ \mathrm{Gy}$

$1\ \mathrm{rem} = 1\ \mathrm{cSv} = 10^{-2}\ \mathrm{Sv}$

（注）

1. 表 1 － 5 は「国際単位系」第 5 版，国際度量衡局 1985 年刊行による。ただし，1 eV および 1 u の値は CODATA の 1986 年推奨値によった。
2. 表 4 には海里，ノット，アール，ヘクタールも含まれているが日常の単位なのでここでは省略した。
3. bar は，JIS では流体の圧力を表わす場合に限り表 2 のカテゴリーに分類されている。
4. EC 閣僚理事会指令では bar，barn および「血圧の単位」mmHg を表 2 のカテゴリーに入れている。

換　算　表

力	N(=10^5dyn)	kgf	lbf
	1	0.101972	0.224809
	9.80665	1	2.20462
	4.44822	0.453592	1

粘　度　1 Pa·s(N·s/m^2) = 10 P(ポアズ)(g/(cm·s))

動粘度　1 m^2/s = 10^4St(ストークス)(cm^2/s)

圧力	MPa(=10 bar)	kgf/cm^2	atm	mmHg(Torr)	lbf/in^2(psi)
	1	10.1972	9.86923	7.50062×10^3	145.038
	0.0980665	1	0.967841	735.559	14.2233
	0.101325	1.03323	1	760	14.6959
	1.33322×10^{-4}	1.35951×10^{-3}	1.31579×10^{-3}	1	1.93368×10^{-2}
	6.89476×10^{-3}	7.03070×10^{-2}	6.80460×10^{-2}	51.7149	1

エネルギー・仕事・熱量	J(=10^7 erg)	kgf·m	kW·h	cal(計量法)	Btu	ft·lbf	eV
	1	0.101972	2.77778×10^{-7}	0.238889	9.47813×10^{-4}	0.737562	6.24150×10^{18}
	9.80665	1	2.72407×10^{-6}	2.34270	9.29487×10^{-3}	7.23301	6.12082×10^{19}
	3.6×10^6	3.67098×10^5	1	8.59999×10^5	3412.13	2.65522×10^6	2.24694×10^{25}
	4.18605	0.426858	1.16279×10^{-6}	1	3.96759×10^{-3}	3.08747	2.61272×10^{19}
	1055.06	107.586	2.93072×10^{-4}	252.042	1	778.172	6.58515×10^{21}
	1.35582	0.138255	3.76616×10^{-7}	0.323890	1.28506×10^{-3}	1	8.46233×10^{18}
	1.60218×10^{-19}	1.63377×10^{-20}	4.45050×10^{-26}	3.82743×10^{-20}	1.51857×10^{-22}	1.18171×10^{-19}	1

1 cal = 4.18605 J（計量法）
　= 4.184 J　（熱化学）
　= 4.1855 J（15 °C）
　= 4.1868 J（国際蒸気表）

仕事率　1 PS（仏馬力）
　= 75 kgf·m/s
　= 735.499 W

放射能	Bq	Ci
	1	2.70270×10^{-11}
	3.7×10^{10}	1

吸収線量	Gy	rad
	1	100
	0.01	1

照射線量	C/kg	R
	1	3876
	2.58×10^{-4}	1

線量当量	Sv	rem
	1	100
	0.01	1

（86 年 12 月 26 日現在）

ANALYSIS OF THE HTTR'S BENCHMARK PROBLEMS AND COMPARISON BETWEEN THE HTTR AND THE FZJ CODE SYSTEMS